Effect of Pulsed Electric Field on Large-Current Toroidal Plasmas

低qトロイダルプラズマに対するパルス誘導電場の影響

渡部政行

Effect of Pulsed Electric Field on Large-Current Toroidal Plasmas

Effect of Pulsed Electric Field on Large-Current Toroidal Plasmas

Doctor Thesis by
Masayuki Watanabe

Directed by
Professor Nobuyuki Inoue
Associate Professor Yuichi Ogawa
and
Associate Professor Zensho Yoshida

A Thesis Submitted to the Division of Engineering,
the Graduate School of the University of Tokyo,
as the Partial Fulfillment for the Requirements
of the Degree of Doctor of Engineering.

Department of Quantum and Systems Science,
Faculty of Engineering
University of Tokyo,
7-3-1 Hongo, Bunkyo-Ku, Tokyo, 113 Japan
1994

Preface

The entropy increases in a microcanonical ensemble, and the most probable state achieves the statistical uniformity. Therefore an ordered structure disappears. When there exists an energy source and an appropriate dissipation process opens up an effective channel of energy flow, so-called '*Self-Organization*' occurs. Self-organization process plays an essential role in many nonlinear system of plasmas. The mechanism of generation of magnetic fields of the earth and other planets are called the 'dynamo'. The dynamo is a spontaneous conversion of the thermal and fluid-dynamic energies into the magnetic energy, and it self-organizes an ordered(simple) structure of magnetic field.

This thesis is devoted to an experimental study of the self-organization process and dynamo activity in a magnetohydrodynamic plasma for controlled thermo-nuclear fusion research. The reversed field pinch (RFP) and ultra-low q (ULQ) configurations are toroidal current carrying systems for magnetic confinement fusion. RFP and ULQ plasmas are interesting not only for the fusion research but also for plasma physics, since the self organization process occurs in both configurations. Plasmas relax spontaneously into a state of minimum energy accompanying plasma instabilities. Finally the plasma is self-stabilized against instabilities, especially the m=1 global kink mode, the internal magnetic field is dominated by dynamo electric field.

To investigate the characteristic of the self-organization process and the dynamo activity, toroidal and poloidal pulsed electric fields have been applied on ULQ and RFP plasmas. In these experiments, synchronized to the pulsed electric fields, various responses of plasma parameters are observed. The internal magnetic field structure and fluctuations have been analyzed. The plasma has a preferential magnetic field structure, and the external perturbations activate fluctuations to maintain the structure through the dynamo effect. This process changes the total dissipation in the system, showing that the self-organization accompanies an enhanced dissipation.

I should mention that this thesis was accomplished with a great helps of the following Professors, advisers, friends,...

I am particularly grateful to Professor Nobuyuki Inoue, Associate Professor Yuich Ogawa and Associate Professor Zensho Yoshida to give me a great chance of study at University of Tokyo. First, I would like to express my appreciation to Professor N.Inoue for his helps over the course of study. His physical advice and discussions are important of my work and his fruitful information of fusion research informed me what is hot topics. Associate Professor Z.Yoshida has instructed me extensively with his physical advice. His suggestion are essential to this work. Without his advice this work has been much more difficult. I am also grateful to Associate Professor Y.Ogawa for his helps, advice and discussions regarding my experimental and theoretical questions. I have contrived to my study owing to his exact advice and daily discussions.

I am grateful to Dr.H.Nihei, Mr.J.Morikawa, Dr.S.Iyengar (Saha institute of Nuclear Physics, India) for their theoretical advice and discussions, and Ms E.Kataoka for her supports kindly. In particularly, I appreciate Mr.J.Morikawa's advice and helps to execute experiments. I also thank Dr.S.Iyengar for discussions concerning REPUTE-1 compression experiment.

I am grateful to Associate Professor K.Yokoyama, Dr.K.Saito, Professor Y.Nogi, Dr.T.Takahashi, Dr.S.Simamura, Professor S.Shiina, Professor S.Hamada and Dr.Osanai at Nihon University for their advice. Associate Professor K.Yokoyama lets me in the field of interesting plasma physics. I would like to thank Dr.K.Saito and Dr.Osanai for their helps and collaborations on analysis of data of ATRAS RFP.

I wish to thank Mr.S.Takeji and Dr.J.Wang for the collaborations. I am grateful to Mr.T.Suzuki, Mr.J.Miyazawa, Mr.K.Sasaki, Mr.S.Kido, Mr.H.Nakanishi, Mr.K.Demachi, Mr.Y.Okamura and Mr.T.Sakurai for technical supports in REPUTE experiment. In particularly I wish to thank to Mr. K.Sasaki, Mr. S.Kido and Mr. H.Nakanishi for helps of numerical analysis and discussions. I am also grateful to Mr. T.Yamamoto, Mr. N.Akiyama and Mr. K.Muto for helps and discussions. I wish to express my thank to all others of the current and former members of Nihon University and University of Tokyo.

Finally I would like to express my thanks to my family, in particularly, my parents who have been supporting my study every time.

Tokyo, December 1994

Masayuki Watanabe

Contents

Chapter 1

INTRODUCTION

1.1 *Toroidal Plasma Experiments for Fusion Research*

This paper describes the 'self-organization process' and 'dynamo activity' in a plasma for controlled thermo-nuclear fusion research. There are two ways to confine a plasma within a cold bottle, one is the inertia confinement and the other is the magnetic confinement. The basic requirement to achieve a fusion reactor is to keep a high temperature plasma detached from a cold wall.

In the magnetic confinement fusion research, the most effective configuration is tokamak [1, 2, 3, 4, 5, 6, 7, 8]. The tokamak is a toroidal current carrying system, where the plasma is confined by a relatively strong toroidal magnetic field generated by external coils, and week poloidal magnetic field generated by a current flowing inside the plasma; see Fig.1.1. A important parameter of plasma physics is the safety factor $q_a = aB_t/RB_\theta$, where a is the minor radius, R is the major radius, B_t is the toroidal magnetic field and B_θ is the poloidal magnetic field. The characteristic of tokamak is that q is kept high. Generally in a toroidal confinement system, the safety factor scales the stability of kink instabilities. The other important parameter for fusion is β, which is the ratio of the plasma pressure and the magnetic pressure. The β value scales the economical advantage as well as the stability of pressure-driven instabilities. A tokamak allows a substantial small β.

The reversed field pinch (RFP) and ultra-low q (ULQ) plasmas, which are also members of toroidal magnetic confinement, have been investigated at many laboratories [9, 10, 11, 12, 13, 14, 15]. An essential difference between the tokamak

and RFP is in their q profiles. In the RFP configuration, the toroidal and poloidal magnetic fields have almost same magnitude. The toroidal magnetic field is reversed in the edge region as shown in Fig.1.2, resulting in a strong shear. The plasma produces such reversed field spontaneously through the 'self-reversal' process and maintains the configuration by the dynamo activity [16, 17, 18, 19]. The dynamo effect produces and sustains a specific magnetic configuration by converting thermal, mechanical or electro-magnetic energy, which will be discussed section 2.1 in detail. The RFP plasma is a interesting subject not only for fusion research but also for plasma physics. Self-reversal and self-generation processes in RFP will be discussed in section 2.2.

The ULQ plasma is a close cousin of RFP. The dynamo activity plays an important role in formation and maintain the ULQ configuration. The ULQ configuration is characterized by $0 < q < 1$, and hence it lies in the intermediate region between tokamak and RFP. Schematic drawing of radial distribution of q profiles for tokamak, ULQ and RFP is shown in Fig.1.3. The ULQ has pitch minimum in the edge [20, 21, 22, 23, 24].

In both RFP and ULQ configurations, the plasma is considered to relax into a minimum energy state through the exciting instabilities. These configurations are self-stabilized against kink modes through nonlinear effect. J.B.Taylor [25, 25] introduced a heuristic model of such relaxation phenomena using the concept of helicity. The theory of magnetic relaxation and its relation to the dynamo activity and kink modes will be discussed in section 2.2.1.

1.2 *Space Plasma Physics*

The mechanism of generation and conservation of astronomical magnetic fields has been a long-standing subject of space plasma physics. The history of the dynamo theory goes back to the magnetic field of the Earth, Sun and other cosmical object.

1.2.1 *Terrestrial magnetism*

The most familiar of dynamo effect is magnetic field of the earth. It was well known the magnetic field of the Earth is dipole but the mechanism is still unresolved.

Consider a conducting fluid under the nucleus of the Earth. Its rotation becomes faster as the distance from the axis increases. Such a differential rotation plays an important role in modification of magnetic field. When there is dipole magnetic field through such a planet, toroidal magnetic field is generated by the rotation as shown in Fig.1.4. This toroidal magnetic field is twisted by convection of fluid as shown in Fig.1.5(Coriolis force). The dipole magnetic field is produced by such a helical convection as shown in Fig.1.6.

1.2.2 *Solar Corona*

The outer edge of the sun about 8000km from the photoshere is called the 'chromoshere'. The temperature of the surface of photoshere is about 10^4k, however in the region of chromoshere, temperature increases up to 10^6k. Hydrogen gas is almost ionized to produce the corona. Such high temperature is not explained by heating due to the nuclear reaction in the core of the Sun. In this layer the magnetic Reynolds number is high, because of the high temperature and low density. Charged particles move together with magnetic field lines. The heating mechanism is considered to be due to the magnetic energy dissipation into thermal energy. Similar anomalous heating occurs in RFP and ULQ, which will be discussed in section 1.3.

The layer with several ten million km thickness surrounding the chromoshere is called the corona. In corona region, density is $10^8 \sim 10^{15} cm^{-3}$, temperature is $0.4 \sim 10^4 eV$ and magnetic field is $1 \sim 10^3 G$. In this region, loop structures are observed, which is considered to be generated by magnetic field coming up from the Sun. Loops are twisted up due to the rotation of their footpoint. When the twisted of magnetic field lines exceeds a critical, the loop becomes unstable and the excess magnetic energy is dissipated explosively through a magnetic reconnection, resulting in a solar flare.

1.2.3 *Magnetic Field of the Sun*

The observation of the Sun has been carried out in detail for a long time and a lot of information have been obtained. The origin and generation of the Sun's magnetic field is also considered to be caused by the dynamo effect. The differential rotation of the Sun is a matter of common knowledge, the angular velocity $\omega(\theta)$ at the latitude θ is

$$\omega(\theta) = (2.78 - 0.35\sin^2\theta - 0.44\sin^4\theta) \times 10^{-6} rad/s.$$

The Sun make one revolution in about 26 days on the equator($\theta = 0$). If an angular momentum is conserved, the speed of rotation at the surface is more faster than inside. Such differential rotation, which is so-call 'ω effect' (explain in section 2.1.1), produces the toroidal magnetic field B_t, from the poloidal magnetic field B_p, and magnetic field is increased. On the other hand, the cyclic process due to the convection and Coriolis force produces the poloidal magnetic field B_p, from the toroidal magnetic field B_t, which is called α effect.

1.3 *MHD Fluctuation*

The MHD fluctuation plays an essential role in formation and maintain of ULQ and RFP configurations. MHD relaxation is a process to dissipate an excess of magnetic energy, which is supplied by external magnetic and electric energies, through the exciting fluctuations. In a toroidal plasma with a large plasma current and with a high magnetic Reynolds number, its magnetic field structure is reconstructed by the combination of induced electric field and 'turbulent electric field' due to the magnetic fluctuations. When the fluctuation grows, the relaxation occurs intermittently or continuously [27]. An example of the intermittent behavior is the sawtooth oscillations, which is usually driven by internal kink instability [28, 29, 30, 31], and an example of the continuous behavior is the turbulent dynamo effect in RFP and ULQ plasmas [16, 17, 18, 19]. The 'turbulent electric field' is here the 'dynamo electric field'.

That magnetic structure is formed the 'force free field'. In the force free field, the magnetic field is everywhere parallel to the current density, resulting in Lorentz force is zero. Some characteristics of the force free field are discussed in section 2.1.1. Such concepts of the force free field was applied to RFP by J.B.Taylor [25, 25]. The characteristic in RFP and ULQ plasmas will be discussed in section 2.2.

In ULQ and RFP, anomalous behaviors are observed due to the dynamo effect. One of the observations is anomalous plasma resistance. The effective resistivity η^* estimated by loop voltage V_l and plasma current I_p, is in the order of $10 \sim 100[\mu\Omega \cdot m]$ for typical ULQ plasmas. While the electron temperature T_e, measured by Thomson scattering, is about 100eV at the center. The classical resistivity η_s is in the order of $1[\mu\Omega \cdot m]$. The resistance anomaly is high : $\eta^*/\eta^s > 10 \sim 10^2$.

An excess of plasma energy is induced by extra toroidal electric field. Such a extra of plasma energy is released through the relaxation process spontaneously. The excess of magnetic energy is dissipated through the exciting fluctuations to ion and electron. For example in present ULQ and RFP plasmas, the observed ion temperature is comparable to or higher than the electron temperature (ULQ, [16, 33, 34] : RFP, [16, 17, 18, 19]). In ULQ experiments such ion heating is burst together with the enhancement of plasma fluctuations in Fig.1.7. These experimental results of spontaneous heating are considered as the same behavior of the Solar flare.

1.4 *Electric Field Drive Experiments*

Force free field is formed in RFP and ULQ configurations. Generally in the toroidal current carrying systems, toroidal magnetic field is generated by external coils and poloidal magnetic field created by plasma current flowing inside the plasma as shown in Fig.1.1. The magnetic field lines are twisted. In such system, induced electric field is only toroidal electric field, and plasma current density is not parallel to magnetic field lines, because the poloidal component of electric field is almost zero in quasi-steady state. In RFP and ULQ plasmas there exists the poloidal electric field, which is driven by plasma fluctuations and plasma current density becomes

parallel to the magnetic field line.

To investigate the characteristic of the turbulent electric field, toroidal and poloidal additionally-pulsed electric fields are induced in RFP and ULQ plasmas. At first, the poloidal electric field is induced by a fast change of the toroidal magnetic field. In this experiment, we can perform two different experiments. These experiments are distinguished between increase or decrease of the toroidal magnetic field. In the case when the toroidal magnetic field rapidly decreases, the direction of externally-induced poloidal electric field is the same with that of turbulent electric field, as shown in Fig.1.8.

At second experiment, a fast rising of the toroidal magnetic field is applied during ULQ discharge, where the direction of the induced poloidal electric field is opposite to that of turbulent electric field, as also shown in Fig.1.8.

In these experiments, we expect that poloidal magnetic field is converted by the induced toroidal magnetic field through the dynamo effects. Moreover the experiment of a fast rising of the toroidal magnetic field, we expect the effect of magnetic compression as well as compression experiments at the conventional tokamaks [35, 36, 37, 38].

At third, the pulsed toroidal electric field is applied due to the additional rising of the toroidal loop voltage, during RFP discharge as shown in Fig.1.9. In this experiments, the poloidal magnetic field increases, because plasma current is increased, and we expect the production of the toroidal magnetic field, converted through the dynamo effect.

In these experiments, we can investigate the transient phases when the twisted magnetic field lines relax or fasten. The motivation of these experiments and experimental results are discussed in chapter 3.

1.5 *Large Kink Behavior*

Kink mode is the instability which is driven by plasma currents. The plasma column is modified when this mode occurs. Figure 1.10(a)(b) shows the modification

of plasma column due to the m=1 and m=2 modes, where m is the azimuthal wave number as shown in Fig.1.11. The basic kink instability is m=1 kink mode. In tokamak, kink mode is the most strong and dangerous instability and sometime plasma discharge is terminated by the enhancement of this mode. Kink mode are usually subdivided into two categories of external kink and internal kink modes. The external kink mode destroys the plasma column and plasma discharge is terminated, while internal kink mode modifies the internal magnetic field structure and the energy loss occurs.

However, these modes are effective for plasma formation in RFP and ULQ configurations. Formation and maintaining in the RFP and ULQ configurations are regarded as the self-organization process in high temperature plasmas. The nonlinear coupling of the kink mode plays essential roles in relaxation and plasma confinement. Both configurations, the internal magnetic profile is dominated by self-organization process through the self stabilization of the kink instabilities. Such behavior will be reviewed in section 2.2 theoretically and the experimental results will be discussed in chapter 5.

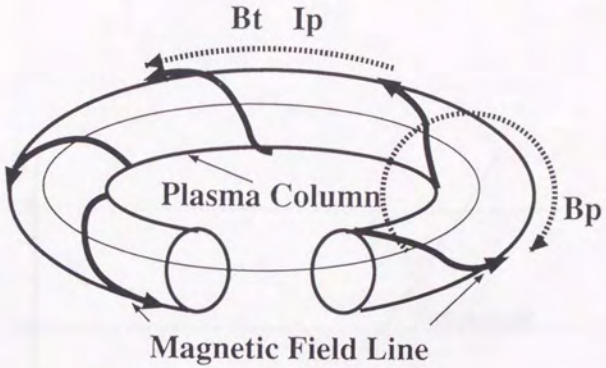

Figure 1.1: Toroidal current carrying system.

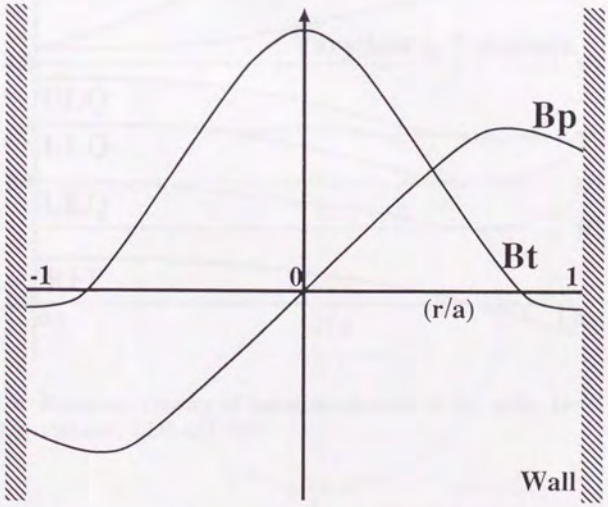

Figure 1.2: Schematic drawing of radial distribution of the magnetic field on RFP configuration.

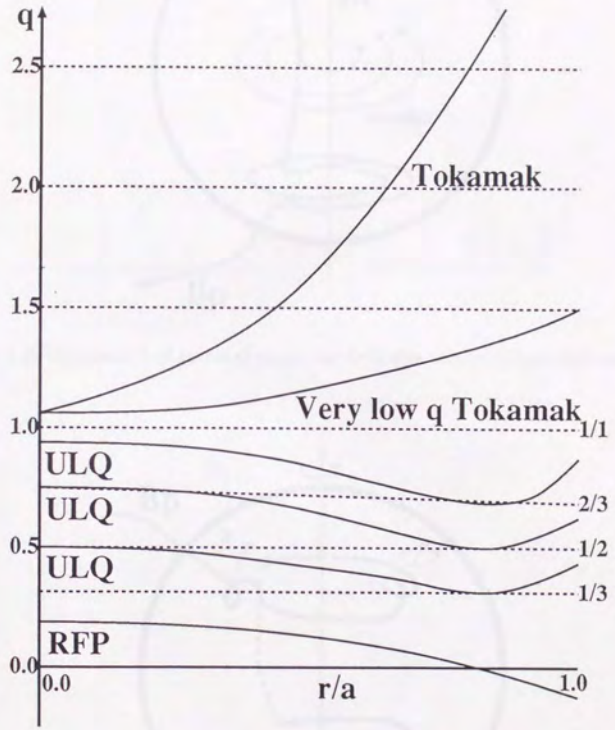

Figure 1.3: Schematic drawing of radial distribution of the safety factor profiles classified by tokamak, ULQ and RFP.

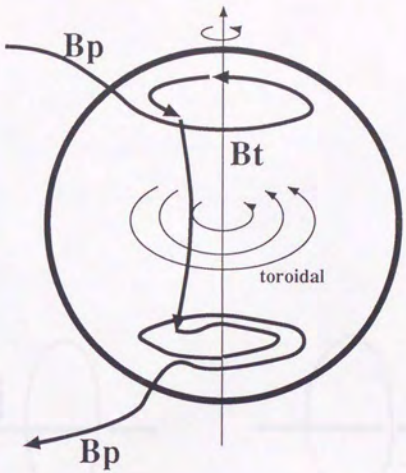

Figure 1.4: Generation of toroidal magnetic field due to the differential rotation.

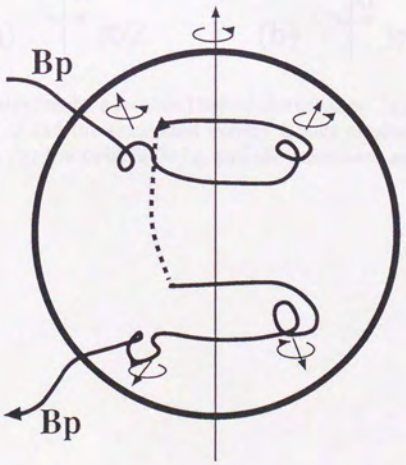

Figure 1.5: Generation of poloidal magnetic field due to the helical convection.

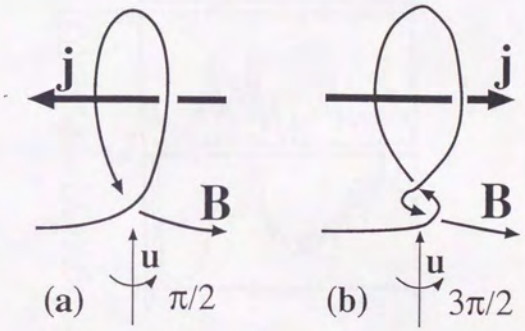

Figure 1.6: Field distortion by a localized helical disturbance. (a) In the loop twisted through an angle $\pi/2$ and the associated current is anti-parallel to magnetic field. On the other hand, (b) the twist is $3\pi/2$, and the associated current is parallel to magnetic field.

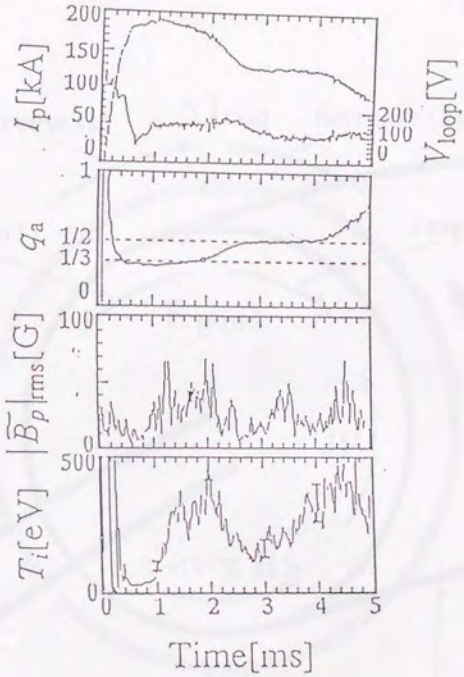

Figure 1.7: Temporal development of ion temperature T_i, and fluctuation of poloidal magnetic field.

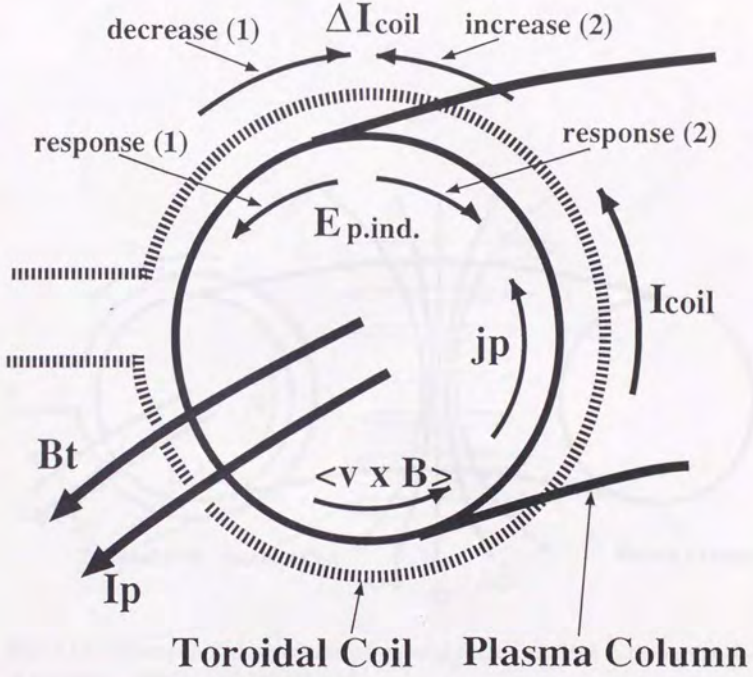

Figure 1.8: Schematic drawing of the induced external poloidal electric field due to a fast change of the toroidal magnetic field. In the case of decrease of the toroidal magnetic field rapidly (decrease(1)), the direction of the external poloidal electric field is the same with that of dynamo electric field,$< v \times B >$,(response(1)). While in the case of increase of the toroidal magnetic field (increase(2)), the direction of the external poloidal electric field is the opposite to that of dynamo electric field (response(2)).

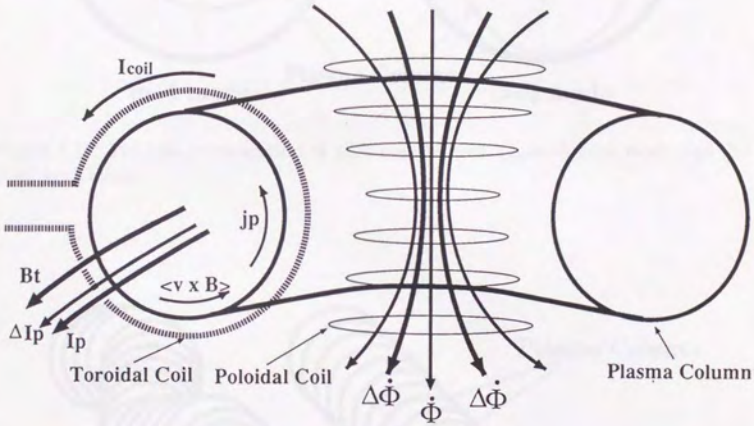

Figure 1.9: Schematic drawing of induced toroidal electric field due to the application of additional toroidal loop voltage ($\Delta\dot{\Phi}$).

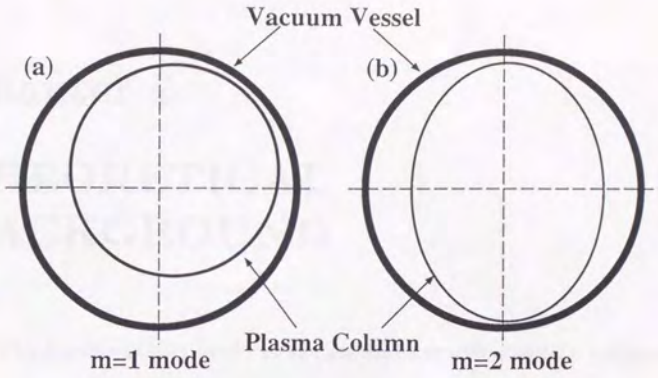

Figure 1.10: Poloidal cross-section of kink instabilities. (a)m=1 kink mode and (b) m=2 kink mode.

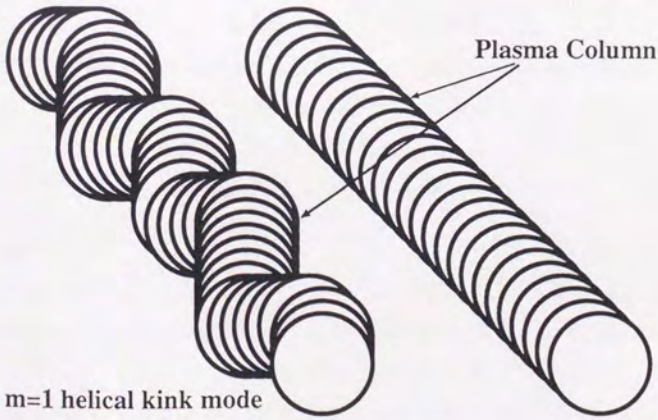

Figure 1.11: The m=1 helical kink instability. The column winds with the magnetic axis.

Chapter 2

THEORETICAL BACKGROUND

The dynamo activity produces and sustains a specific magnetic configuration by converting thermal, mechanical or electro-magnetic energy. Some basic dynamo models and their equations at the space and fusion plasmas are reviewed in this chapter.

2.1 *Dynamo Effect*

2.1.1 *Magnetic Field Diffusion*

The basic MHD equations are written as follows;

$$\begin{aligned} \nabla \times \boldsymbol{E} &= -\frac{\partial \boldsymbol{B}}{\partial t}, \\ \nabla \times \boldsymbol{B} &= \mu_0 \boldsymbol{j}, \\ \nabla \cdot \boldsymbol{B} &= 0, \end{aligned} \tag{2.1}$$

where $\boldsymbol{B}$ is magnetic flux density, $\boldsymbol{E}$ is electric field, $\boldsymbol{j}$ is electric current density and μ_0 is permeability. General Ohm's law is described as follow;

$$\boldsymbol{E} = \eta \boldsymbol{j} - \boldsymbol{v} \times \boldsymbol{B}, \tag{2.2}$$

where $\boldsymbol{v}$ is the fluid velocity and η is resistivity.

The most familiar behavior of dynamo effect is the generation of the magnetic field. Consider the transition and maintaining of magnetic field on the basis of Equation (2.1),(2.2). For example, the fluid is considered to be well conductive. When such fluid is covered by magnetic field $\boldsymbol{B}$, and it moves in the magnetic field and that velocity of fluid is $\boldsymbol{v}$, the induced electromotive force $\boldsymbol{v} \times \boldsymbol{B}$, is generated. In this fluid, the magnetic field is modified by its motion and this motion influences to itself again through the $\boldsymbol{v} \times \boldsymbol{B}$ electric field. Such a behavior is so-called 'dynamo effect', and it is that conversion from kinetic energy to magnetic energy.

The basic equation showing the change of the magnetic field is written as follow,

$$\frac{\partial \boldsymbol{B}}{\partial t} = \nabla \times (\boldsymbol{v} \times \boldsymbol{B}) + \eta \nabla^2 \boldsymbol{B}. \tag{2.3}$$

In this Equation(2.3), the second term of $\eta \nabla^2 \boldsymbol{B}$, implies the diffusion of magnetic field(damping of magnetic energy), and the first term of $\nabla \times (\boldsymbol{v} \times \boldsymbol{B})$, implies the modification of magnetic field due to the motion of fluid(increase of magnetic energy). The ratio of the first term to the second term is called the magnetic Reynolds number R_m. The condition to grow the magnetic field is $R_m \gg 1$.

Equation(2.3) can not be solved without information of $\boldsymbol{v}$. The method to solve the Equation(2.3) on the assumption of the suitable value of $\boldsymbol{v}$, is called 'Kinematic

dynamo'. On the other hand, the method that the velocity of fluid is given by the following MHD equations,

$$\rho\frac{dv}{dt} = \boldsymbol{F} - \nabla p + \rho g + \boldsymbol{j} \times \boldsymbol{B} + \rho\nu\nabla^2 v,$$

$$\frac{d\rho}{dt} + \nabla \cdot (\rho \boldsymbol{v}) = 0,$$

$$\rho\frac{dU}{dt} = \frac{p}{\rho}\frac{d\rho}{dt} + Q,$$

$$p = (constant.) \times \rho T,$$

is called 'MHD dynamo', where ρ is a mass of fluid, $\boldsymbol{F}$ is the external force, g is gravity, ν is a coefficient of viscosity, U is thermal energy and Q is a heating effect of viscosity, thermal conduction and current.

2.1.2 *Dynamo Effect by Coriolis Force and Convection*

There are some models to explain the origin of the magnetic field at the earth. For example, the model of the modification and growth of magnetic field due to the Coriolis Force and Convection is reviewed. The differential rotation, which is matter of common knowledge, is an important factor for modification of magnetic field. When there is dipole magnetic field into such fluid, magnetic field lines are influenced by this rotation and magnetic field rotates around notational axis as shown in Fig.1.4 (Generation of toroidal magnetic field). This toroidal magnetic field is modified by convection of fluid and twisted by the Coriolis force as shown in Fig.1.5(b) (helical convection). When there are large convection, the dipole magnetic field is produced by composition of helical convection (Fig.1.6).

One of the model, that is given by E.N.Paker [39], is reviewed. The velocity of planet $\boldsymbol{v}$, is considered as the sum of toroidal component $\boldsymbol{v}_\phi$, and poloidal component $\boldsymbol{v}_p$, of velocity,

$$\boldsymbol{v} = \boldsymbol{v}_\phi(\phi) + \boldsymbol{v}_p(r, \theta),$$

hence

$$| \nabla \times (v \times B) |_{\phi} = B_r(\frac{\partial v_\phi}{\partial r} - \frac{v_\phi}{r})e_\phi.$$

One finds from Equation(2.4),

$$\frac{\partial B_\phi}{\partial t} - | \eta \nabla^2 B |_{\phi} = | \nabla \times (v \times B) |_{\phi},$$

hence

$$\frac{\partial B_\phi}{\partial t} - \eta(\nabla^2 - \frac{1}{r^2 sin^2\theta})B_\phi = B_r(\frac{\partial v_\phi}{\partial r} - \frac{v_\phi}{r}). \tag{2.4}$$

On the other hand, poloidal component of Equation(2.4), read from B_p=$\nabla \times$ A, where A is vector potential,

$$\frac{\partial B_p}{\partial t} - | \eta \nabla^2 B |_{p} = | \nabla \times (v \times B) |_{p},$$

$$\frac{\partial A_p}{\partial t} - \eta(\nabla^2 - \frac{1}{r^2 sin^2\theta})A_p = < v_p \times B >_{\phi}, \tag{2.5}$$

where <> indicates the time average, and B_ϕ and B_p are toroidal and poloidal magnetic fields respectively. Equation(2.4) shows the generation of B_ϕ from B_p originated in asymmetrical rotation. Equation(2.5) shows generation of B_p from B_ϕ which is caused by helical convection.

2.1.3 *Turbulent Dynamo*

The origin of dynamo effect is considered to be created not only under the ordered motion but also under the random motion. This dynamo model was constructed by Steenbeck [40] and is called the 'Turbulent dynamo'. The characteristic of Ohm's law(Equation(2.2)) is the current, induced by dynamics of conductive fluid, is perpendicular to the magnetic flux density B.

Let's consider in the case when one of the especial structure is formed. This structure is that current density j is parallel to magnetic flux density B. This effect is called by 'α effect'. When such structure is formed, we can consider the closed process as shown in Fig.2.1, where B_t and B_p are toroidal and poloidal magnetic

fields, respectively and j_t and j_p are toroidal and poloidal current density, respectively. This is the most fundamental mechanism of magnetic dynamo concerning to closed magnetic/current system.

We consider the Ohm's law with turbulent field. When the dynamics of fluid is turbulent, the turbulent electric field $\boldsymbol{E}_T$ takes place. The Ohm's law(2.2) is modified as follows,

$$< \boldsymbol{E} >=< \eta \boldsymbol{j} > - < \boldsymbol{v} \times \boldsymbol{B} > - \boldsymbol{E}_T \tag{2.6}$$

$$\boldsymbol{E}_T =< \tilde{\boldsymbol{v}} \times \tilde{\boldsymbol{B}} > . \tag{2.7}$$

Here $\boldsymbol{E}_T$ is turbulent electric field, $\tilde{\boldsymbol{v}}$ and $\widetilde{\boldsymbol{B}}$ are turbulent components of $\boldsymbol{v}$ and $\boldsymbol{B}$, respectively. In this case it is possible the current flows in parallels with the magnetic flux density. Such a poloidal component of electric field does not exist in general Ohm's law(2.2).

Consider the fluctuating fluid of $\boldsymbol{v}$ and $\boldsymbol{B}$. The corresponding mean fields $(\boldsymbol{v}_0, \boldsymbol{B}_0)$ are defined to be the expectation values of $(\boldsymbol{v}, \boldsymbol{B})$ in an ensemble of identical system, and $(\tilde{\boldsymbol{v}}, \widetilde{\boldsymbol{B}})$ shall be used to denote the difference, $(\boldsymbol{v}\text{–}\boldsymbol{v}_0,\ \boldsymbol{B}\text{–}\boldsymbol{B}_0)$

$$\boldsymbol{v} = \boldsymbol{v}_0 + \tilde{\boldsymbol{v}}$$

$$\boldsymbol{B} = \boldsymbol{B}_0 + \widetilde{\boldsymbol{B}}.$$

From Equation(2.1), we obtain

$$\frac{\partial}{\partial t}(\boldsymbol{B}_0 + \widetilde{\boldsymbol{B}}) = \nabla \times \{(\boldsymbol{v}_0 + \tilde{\boldsymbol{v}}) \times (\boldsymbol{B}_0 + \widetilde{\boldsymbol{B}})\} + \eta \nabla^2 (\boldsymbol{B}_0 + \widetilde{\boldsymbol{B}}).$$

And we obtain

$$\frac{\partial \boldsymbol{B}_0}{\partial t} = \nabla \times (\boldsymbol{v}_0 \times \boldsymbol{B}_0) + \nabla \times \boldsymbol{\varepsilon} + \eta \nabla^2 \boldsymbol{B}_0, \tag{2.8}$$

$$\frac{\partial \widetilde{\boldsymbol{B}}}{\partial t} = \nabla \times (\boldsymbol{v}_0 \times \widetilde{\boldsymbol{B}}) + \nabla \times (\tilde{\boldsymbol{v}} \times \boldsymbol{B}_0) + \nabla \times \boldsymbol{G} + \eta \nabla^2 \widetilde{\boldsymbol{B}},$$

where

$$\varepsilon = < \tilde{v} \times \widetilde{B} >,\ G = \tilde{v} \times \widetilde{B} - \varepsilon. \tag{2.9}$$

Since $\widetilde{B}$ is considered to be linear function of B_o, there is also linear relation between ε and B_o. When the turbulence is homogeneous and isotropic, therefore, Equation(2.8) is rearranged as follow,

$$\frac{\partial B_o}{\partial t} = \nabla \times (v_o \times B_o + \alpha B_o) + \eta \nabla^2 B_o. \tag{2.10}$$

Equation(2.10) is approximated to $\varepsilon = \alpha\ B_o$. Here r,$\phi$,z describe the cylindrical coordinate system, v_o, B_o and ε are described as follows,

$$\begin{aligned} v_o &= r\omega(r,z)e_\phi + V_p, \\ B_o &= B(r,z)e_\phi + B_p, \\ \varepsilon &\doteq \varepsilon_\phi e_\phi + \varepsilon_\phi = \alpha B e_\phi + \alpha B_p, \end{aligned}$$

and

$$B_p = \nabla \times A(r,z)e_\phi.$$

Hence, Equation(2.11) is rearranged as follows,

$$\frac{\partial B_t}{\partial t} + r(V_p \cdot \nabla)(r^{-1}B) = r(B_p \cdot \nabla)\omega + \nabla \times (\alpha B_p) + \eta(\nabla^2 - r^{-2})B, \tag{2.11}$$

$$\frac{\partial A}{\partial t} + r^{-1}(V_p \cdot \nabla)(rA) = \alpha B_t + \eta(\nabla^2 - r^{-2})A, \tag{2.12}$$

Equation(2.11) implies that B_t, is generated by B_p by the differential rotation (ω effect ; the first term of right side of equation) and helical convection(α effect ; the second term of right side of equation). Equation(2.12) implies that B_p, is generated by B_t, by the helical convection(α effect ; the first term of right side of equation). The combination of ω effect in Equation(2.11) and α effect in Equation(2.12) is called '$\alpha\omega$-dynamo'. On the other hand, α effect in Equation(2.11) and α effect in Equation(2.12) is called 'α^2-dynamo'.

2.2 *Self-Organization*

2.2.1 *Magnetohydrodynamic Relaxation*

Helicity Concept and its Conservation

Plasma is regarded as a perfectly conducting fluid without resistivity and any acceptable magnetic field must satisfy the condition $\nabla \cdot B = 0$. Any variation of the fluid must be with the constraint

$$\frac{\partial B}{\partial t} = \nabla \times (v \times B). \tag{2.13}$$

This equation implies that the topology of system is conserved any modification of magnetic field and magnetic field lines are frozen into the plasma. J.B.Taylor has shown that equation(2.13) can be replaced by an infinite set of integral constraints involving the magnetic helicity K is defined by

$$K = \int_{\psi} A \cdot B dr, \tag{2.14}$$

Where the integration is carried out over the volume enclosed by any flux surface ψ. This concept of magnetic helicity is an essential for understanding of invariable topology of plasma. This concept was used by Woltjer [41],Wells and Norwood [42] and Chandrasekhar [43] for the space plasma and applied to fusion plasmas by work of Taylor [25, 44, 45].

Since plasma is regarded as perfectly conducting fluid, the magnetic helicity K is invariant and is replaced the single invariant of the flexible wire loop. This indicates invariant of the topology of magnetic field. For example when two magnetic flux tubes, which magnetic flux are ψ_1 and ψ_2 respectively, are cross each other as shown in Fig.2.2, we obtain K as follow

$$K = \pm 2\psi_1\psi_2$$

One closed field line links other n times in perfectly conducting fluid, the two loops must remain linked n times through any plasma motion.

Kinetic and Potential Energy of the Plasma and Magnetic Field

The total kinetic and potential energy of the plasma, W_0 is given by

$$W_0 = \int (\frac{1}{2}\rho v^2 + \frac{p}{\gamma - 1} + \frac{B^2}{2\mu_0}) d\boldsymbol{r}, \tag{2.15}$$

where ρ is mass density. As the plasma turbulent involves with its initial state, it dissipates energy through thermal contract with the wall or thermal and particle diffusions. Finally equation(2.15) is reduced to only the term of magnetic energy

$$W = \frac{1}{2\mu_0} \int B^2 d\boldsymbol{r}, . \tag{2.16}$$

Taylor Theory and Magnetic Reconnection

Consider the perfectly conducting plasma, where plasma resistivity is zero. Where vector potential $\boldsymbol{A}$ is defined by $B = \nabla \times \boldsymbol{A}$, equation (2.13) is reduces to

$$\boldsymbol{B} \cdot \frac{\partial \boldsymbol{A}}{\partial t} = \nabla \cdot (\chi B),$$

where χ is arbitrary gauge.

Hence

$$\int \boldsymbol{B} \cdot \frac{\partial \boldsymbol{A}}{\partial t} \boldsymbol{r} = \int \nabla \cdot (\chi B) d\boldsymbol{r} = \chi \oint B \cdot n d\boldsymbol{r} = 0,$$

where n is a normal unit vector.

Consider the time differential magnetic helicity as follow,

$$\frac{d\boldsymbol{K}}{dt} = \int \frac{\partial}{\partial t} (\boldsymbol{A} \cdot \boldsymbol{B}) d\boldsymbol{r} = 2\eta \int \boldsymbol{j} \cdot \boldsymbol{B} d\boldsymbol{r} = 0, \tag{2.17}$$

where η is plasma resistivity and $\boldsymbol{j}$ is plasma current density. Thus magnetic helicity is conserved on condition that plasma is perfectly conducting.

Subsequently, consider the condition that minimum of the magnetic helicity as variation of vector potential $\delta \boldsymbol{A}$. We obtain

$$\delta W = \int (\delta \boldsymbol{A} \cdot \frac{\nabla \times \boldsymbol{B}}{\mu_0}) d\boldsymbol{r} = \frac{1}{2\mu_0} \int 2\delta \boldsymbol{B} \cdot \boldsymbol{B} d\boldsymbol{r},$$

$$\delta K = 2 \int (\delta \boldsymbol{A} \cdot \boldsymbol{B}) d\boldsymbol{r} = \int (\delta \boldsymbol{A} \cdot \boldsymbol{B} + \boldsymbol{A} \cdot \delta \boldsymbol{B}) d\boldsymbol{r}.$$

Calculate the magnetic energy minimum state on condition of constraint of equation(2.17) using Lagrange multiplier λ

$$\delta W + (\frac{\lambda}{2\mu_0})\delta K = \frac{1}{\mu_0}\int \delta \boldsymbol{A}(\nabla \times \boldsymbol{B} - \lambda \boldsymbol{B})d\boldsymbol{r} = 0,$$

hence, we can obtain the Equation(2.18) as follow

$$\nabla \times \boldsymbol{B} = \lambda \boldsymbol{B}. \tag{2.18}$$

This equation implies that plasma current density is paralleled to magnetic field line, because $\nabla \times \boldsymbol{B} = \mu_0 \boldsymbol{j}$. This equation indicates the condition of the force free field.

Finely, plasma is regarded as a conducting fluid with small resistivity surrounding the perfectly conducting shell. Turbulence with a small resistivity can allow the plasma rapid access to particular minimum energy state. In this case it is possible that the cutting off or reconnection of the magnetic field lines occurs. However in the case that plasma resistivity is small enough, that is time variation of magnetic helicity K is more shorter than time variation of magnetic energy W,

$$|\frac{dK}{dt}| \ll |\frac{dW}{dt}|.$$

The consideration of relaxation process, surrounding the perfectly conducting shell, becomes 'the consideration of minimum state of magnetic energy include the boundary condition with constant K'. In this case, similar to perfectly conducting plasma, we can obtain

$$\nabla \times \boldsymbol{B} = \mu \boldsymbol{B}, \tag{2.19}$$

where μ is a constant determined by K and the boundary conditions.

This process is one of the self-organization and involves the reconnection of magnetic field lines. From equation(2.19) we can also understand that plasma current density $\boldsymbol{j}$ is parallel to magnetic flux density $\boldsymbol{B}$ and this condition is the force free field, as discussed in section 1.3.

Non-linear Effect of Kink Mode

We consider here the correlation of self-organization process and dynamo effect. In toroidal current carrying system, there are two type dissipation processes. One is the classical resistive diffusion of magnetic field, and the other is MHD relaxation, accompanied with m=1 kink instability. For examples of sawtooth oscillations [28, 29, 30, 31] and self-organization process [16, 17, 18, 19]. In resent experimental [46, 47], numerical [48, 49], and theoretical [50, 51, 52] research, the growth of the m=1 global kink mode is the key of MHD relaxation. 3-D simulation study on RFP plasma and experimental studies with magnetic fluctuations it become clear the mechanism of MHD relaxation process.

2.2.2 *RFP Configuration*

The theoretical and experimental research on RFP has been performed. The RFP is a member of the toroidal pinch system. The essential feature of RFP configuration is the toroidal magnetic field reverses on the outside of the plasma. In this section the dynamo effect in RFP plasma is reviewed.

One of the interesting behavior of RFP plasma is the generation of toroidal magnetic field spontaneously [16, 17, 18, 19]. For example the toroidal flux inside of the reversal surface, ψ, is written by

$$\frac{\partial \psi}{\partial t} = \frac{2\pi r_0 \eta}{\mu_0} \left. \frac{dB_z}{dr} \right|_{r=r_0} < 0. \tag{2.20}$$

This Equation(2.20) indicates that RFP configuration diffuses due to the plasma resistance. In present RFP experiments, it has been found that plasma duration is sustained for a long period compared with the magnetic diffusion time ($\tau_R = \mu_0 a^2/\eta$, where μ_0 is the magnetic permeability, a is the plasma minor radius and η is the plasma resistivity) [54, 55, 56, 57]. This result implies that there is a mechanism which the B_t, is generated due to the dynamo effect. If the plasma current can be held, plasma discharge is maintained due to the generation of the toroidal magnetic field.

Such RFP configuration can be described to a first approximation by theory of 'magnetic relaxation' due to J. B. Taylor [25, 58], as discussed in section 2.2. According to this theory, this magnetic field configuration is force-free field, and satisfies the equation (2.19). In cylindrical coordinate, an analytical solution of equation(2.19) can be obtained the so-called Bessel Function Model (BFM) given by,

$$\begin{aligned} B_z &= B_0 J_0(\mu r), \\ B_\theta &= B_0 J_1(\mu r). \end{aligned} \tag{2.21}$$

This equation implies B_z reverses in the outer region, $\mu r > 2.405$. Those configurations have two main parameters, which describes plasma conditions.

$$\textit{Pinch Parameter} \quad ,\theta = \frac{B_p(a)}{<B_t>}$$

$$\textit{Reversal Parameter} \quad ,F = \frac{B_t(a)}{<B_t>},$$

From Equation(2.21), F and θ is reduced to

$$\begin{aligned} \theta &= \frac{\mu a}{2}, \\ F &= \frac{\mu a J_0(\mu a)}{2 J_1(\mu a)}. \end{aligned} \tag{2.22}$$

We can obtain,

$$F = \frac{\theta J_0(2\theta)}{J_1(\theta)}. \tag{2.23}$$

Figure 2.3 shows the theoretical $F - \theta$ diagram.

2.2.3 *ULQ Configuration*

The ULQ plasma is close cousin RFP, and is also a toroidal current carrying system with the $0 < q < 1$. The different as compared with RFP plasma is that the toroidal magnetic field is not reversed on the outside of plasma. In present ULQ experiments, similar to RFP, it has been found that plasma duration is sustained a long period as compared with the magnetic diffusion time, because of the mechanism of self-generation of toroidal magnetic field [16].

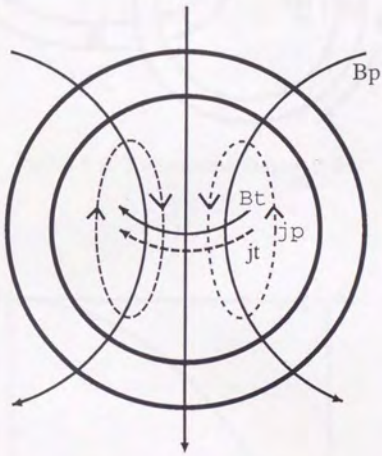

Figure 2.1:
A possible self-maintaining magnetic field configuration in an electrically conducting sphere with α mechanism. The magnetic field $\boldsymbol{B}$, is axisymmetric. It is composed of a poloidal part $\boldsymbol{B}_p$, with the field line in the meridional planes and a toroidal magnetic field $\boldsymbol{B}_t$, with the line encircling the axis of symmetry. Due to the α effect, $\boldsymbol{B}_t$ drives a toroidal current $\boldsymbol{j}_t$. This current $\boldsymbol{j}_t$, is accompanied by the poloidal magnetic field $\boldsymbol{B}_p$, which drives a poloidal current $\boldsymbol{j}_p$, accompanied by the toroidal magnetic field $\boldsymbol{B}_t$.
$j_t \Rightarrow B_t(\alpha \text{ effect}) \Rightarrow j_p(Ampere'law) \Rightarrow B_p(\alpha \text{ effect}) \Rightarrow j_t(Ampere'law) \Rightarrow$,

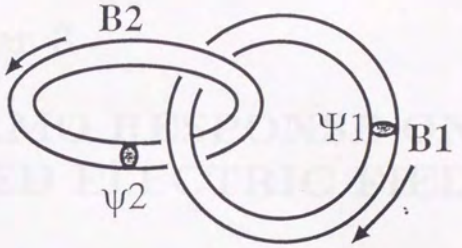

Figure 2.2: Two crossed magnetic flux.

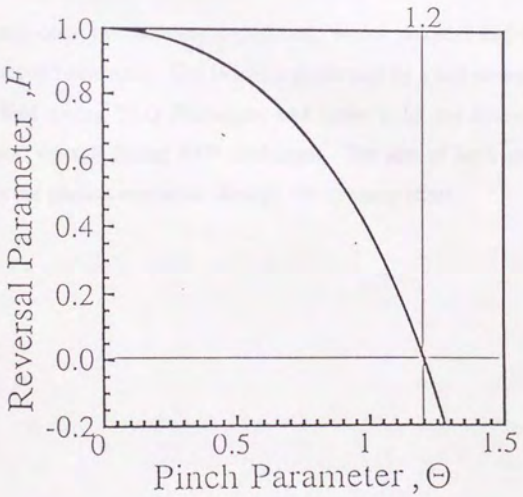

Figure 2.3: Theoretical $F - \theta$ diagram.

Chapter 3

DYNAMO RESPONSE ON PULSED ELECTRIC FIELD

The dynamo effect is introduced in chapter 2. In this chapter the responses of ULQ and RFP plasmas on an induced pulse electric field are discussed experimentally.

We have done two different experiment, where poloidal and toroidal electric fields are applied externally. The former is performed by a fast change of the toroidal magnetic field during ULQ discharges, and latter is by the secondary rise of the toroidal loop voltage during RFP discharges. The aim of both experiments is to investigate the plasma responses through the dynamo effect.

3.1 *Averaged Ohm's Law with Externally-Driven Electric Field*

3.1.1 *Averaged General Ohm's Law*

Here we consider, for example, the turbulent field $\boldsymbol{F}$, and defines the mean field $<\boldsymbol{F}>$ as the expectation value of $\boldsymbol{F}$ in an ensemble of identical system and the fluctuation $\widetilde{F}$ as the difference from the mean field. The following relations, the Reynolds relations, hold

$$\boldsymbol{F} =< \boldsymbol{F} > +\widetilde{F},$$

$$< \widetilde{F} >= 0,$$

$$< \boldsymbol{F} + \boldsymbol{G} >=< \boldsymbol{F} > + < \boldsymbol{G} >,$$

$$<< \boldsymbol{F} > \cdot \widetilde{G} >= 0.$$

Let us consider a generalized Ohm's law(Equation(2.2)) given by

$$< \boldsymbol{E} >=< \eta \boldsymbol{j} > - < \tilde{\boldsymbol{v}} \times \widetilde{\boldsymbol{B}} > . \tag{3.1}$$

Hence, the toroidal and poloidal components of Ohm's law are given as follows,

$$\begin{aligned} < \eta \boldsymbol{j} >_t &= < \boldsymbol{E} >_t + < \boldsymbol{E}_D >_t \ , \\ < \eta \boldsymbol{j} >_p &= < \boldsymbol{E} >_p + < \boldsymbol{E}_D >_p \ , \end{aligned} \tag{3.2}$$

where $< \boldsymbol{E} >_t$ and $< \boldsymbol{E} >_p$ are externally-induced toroidal and poloidal electric fields, respectively, and E_D defined by $< \tilde{\boldsymbol{v}} \times \tilde{\boldsymbol{B}} >$ is an electric field by fluctuations. Since the poloidal component of externally-induced electric field $< \boldsymbol{E} >_p$, becomes almost zero [48] in the quasi-steady state, the poloidal current, which is required to form the force free minimum energy state $\nabla \times \boldsymbol{B} = \lambda \boldsymbol{B}$, is sustained by the turbulent electric field $< \boldsymbol{E}_D >_p$, through the MHD instabilities and/or fluctuations. Here the time averaged Ohm's law with turbulent fields is reduced to,

$$\begin{aligned} < \eta \boldsymbol{j} >_t &= < \boldsymbol{E} >_t + < \boldsymbol{E}_D >_t \ , \\ < \eta \boldsymbol{j} >_p &= \quad\quad + < \boldsymbol{E}_D >_p \ . \end{aligned} \tag{3.3}$$

If the pulsed toroidal or poloidal electric fields are applied externally, it is expected the plasma characteristics might spontaneous changes through the $< \boldsymbol{E}_D >$.

3.1.2 *Averaged Ohm's Law with Externally Induced Poloidal Electric Field*

To investigate the characteristic of force free field, the externally-induced poloidal electric field is applied on the ULQ plasma. Such externally-poloidal electric field is induced by a change (decrease or increase) of the toroidal magnetic field rapidly during plasma discharges, and is added to Ohm's law as follows,

$$\begin{aligned} <\eta j>_t &= <E>_t + <E_D>_t \quad , \\ <\eta j>_p &= \quad\quad + <E_D>_p \pm E_{p.ind.} \quad . \end{aligned} \tag{3.4}$$

The schematic drawing of these components is shown in Fig.1.8. In the case of the decrease of the toroidal magnetic field, the direction of the external poloidal electric field is the same as that of dynamo electric field ($+E_{p.ind.}$). In this experiment, the improvement of the plasma confinement is expected, because dynamo electric field with plasma fluctuations is partly replaced by induced electric field. Such an experiment regards as 'Positive E_p pulsed experiment'.

While, in the case of increase of the toroidal magnetic field, the direction of the external poloidal electric field is opposite to that of dynamo electric field. ($-E_{p.ind.}$). This regards as 'Negative E_p pulsed experiment'. This experiment is identical to so-called minor radius compression, similar to TUMAN's experiment [59].

In these experiments, we investigate the variation of plasma characteristic in transient phase.

3.1.3 *Averaged Ohm's Law with Additionally Induced Toroidal Electric Field*

We consider here the additional toroidal electric field. The toroidal and poloidal components of Ohm's law with the effect of application of additional toroidal electric field are given as follows,

$$\begin{aligned} <\eta j>_t &= <E>_t + <E_D>_t + E_{t.ind.} \quad , \\ <\eta j>_p &= \quad\quad + <E_D>_p \quad . \end{aligned} \tag{3.5}$$

In the case that toroidal electric field is applied additionally in force free field, the toroidal plasma current increases, resulting in the increase of the poloidal magnetic field. In these experiments, we expect the increase of the toroidal magnetic field converted by the induction of the poloidal magnetic field through the dynamo effect.

On applying additional poloidal and toroidal electric field for ULQ and RFP plasmas, the conversion of the magnetic field between toroidal and poloidal components through dynamo effect is studied.

3.1.4 *Anomalous Resistance and Ion Heating*

The plasma resistance anomaly is investigated on ULQ and RFP discharges theoretically and experimentally. The electron temperature T_e, measured by Thomson scattering, is about 100eV at the center in the typical ULQ discharge as shown in Fig.1.7($I_p \sim 200[kA], B_t \sim 0.3[T]$). The classical resistivity η_s, that is so-called the Spitzer resistivity,

$$\eta_s = \frac{\pi e^2 m^{1/2}}{(4\pi\varepsilon_0)^2 (KT_e)^{3/2}} ln\Lambda, \tag{3.6}$$

is in the order of $1[\mu\Omega \cdot m]$, where $ln\Lambda \sim 10$. While, the effective resistivity η^* defined by

$$\eta^* = \frac{V_l}{I_p} \cdot \frac{2R}{a^2}. \tag{3.7}$$

is estimated to be in the order of $10 \sim 100[\mu\Omega \cdot m]$. The measured plasma resistivity is $10 \sim 100$ times as high as the classical Spitzer resistivity. This enhancement of plasma resistance component with Spitzer resistivity is called as the resistance anomaly. This resistance anomaly is considered to be caused by energy and helicity losses accompanied with plasma fluctuations and disagreement between current density profile and plasma resistivity profile as shown in Fig.3.1. In ULQ discharge, the resistance anomaly is also observed, and is that the inversely proportional to the toroidal magnetic field [60] in ULQ configuration as shown in Fig.3.2.

Such extra of plasma energy is released through the relaxation process spontaneously. For example, in present ULQ and RFP plasmas, the observed ion temper-

ature is comparable to or higher than the electron temperature (ULQ, [16, 33, 34] : RFP, [16, 17, 18, 19]). It is clear that ion is heated explosively by the dissipation of magnetic energy. These experimental behavior are considered as the same phenomenon of a Solar flare.

3.2 *Experimental Configuration*

3.2.1 *REPUTE-1 ULQ Experiment*

REPUTE-1 Device (Univ. of Tokyo)

REPUTE-1 is a middle size toroidal pinch device with major and minor radii of R=0.82m and a=0.22m respectively. The flux swing using the iron core makes 1.6 V.sec. The vacuum vessel consists of 1.0mm thick Inconel-625 below and 2.6mm thick port segments toroidally. The resistance of the vessel are $6.5m\Omega$ toroidally and $0.4m\Omega$ poloidally. The vacuum vessel has no cut toroidally and poloidally. A 5mm thick stainless steel shell surrounds the vessel. The time constant of the shell is about 0.25msec for toroidal magnetic field.

Diagnostic Systems

The Rogowski coil wrapped around the vacuum vessel measures the plasma current. The loop voltage V_{loop} is measured from flux loops going toroidally around the vacuum vessel. Two flux loop are wound poloidally around the vacuum vessel to measure the toroidal flux. There are about 100 magnetic pick-up coils located between the vessel and shell to measured B_t, B_p and B_r fields. The MHD fluctuations, plasma position and toroidal and poloidal mode number are measured by these coils. The eight channels fiber visible-light guide system was installed in poloidal cross-section. The interference filter of this system can change easily for various lines ($e.g., H_\alpha, H_\epsilon I, N_\epsilon I, ...$). The schematic drawing of this system and the layout of magnetic probes arrangement are shown in Fig.3.3. Moreover electron temperature is measured by Thomson scattering, line-averaged electron density is

measured by CO_2 interferometer and ion temperature is measured by visible light spectrometer. The layout of main diagnostic systems is shown in Fig.3.4. To obtain a information of variation of internal magnetic structure, magnetic probe arrays is installed. The schematic drawing of magnetic probe array is shown in Fig.3.5. The spatial structures of plasma current density $j(r)$ and safety factor $q(r)$ is estimated.

Toroidal Coil Current and Toroidal Magnetic Field for the Experiments of Induce Poloidal Electric Field

Power for the toroidal magnetic field coil is supplied by 5 groups of capacitor bank, totally 820kJ.

In the case of the reduction of the toroidal magnetic field, the toroidal magnetic field system produces 2.5kG field at the plasma major radius for the bias field and can decrease to negative field with a time constant of 0.3msec. The time evolutions of the toroidal coil current is shown in Fig.3.6(a). This experiment regards as 'Positive E_p pulsed Experiment'.

While, in the case of the rising of the toroidal magnetic field, toroidal power supply produces typically 1kG field and can increase up to 3.5kG field with a time constant of 0.3msec. The time evolutions of the toroidal coil current is shown in Fig.3.6(b). This experiment regards as 'Negative E_p pulsed Experiment'.

Typical REPUTE-1 ULQ Discharge

The operational plasma current is usually in the range of $50 \sim 300kA$. Figure 3.7 shows the typical 200kA ULQ discharge. The figure shows the plasma current I_p, one turn voltage V_{loop}, averaged toroidal magnetic field $< B_t >$, safety factor at the wall q_a, the center chord averaged electron density $\overline{n_e}$, pinch parameter θ, reversal parameter F, and magnetic fluctuation. The stepwise decrease of plasma current, accompanied with enhancement of loop voltage and plasma fluctuations, has been observed. This stepwise phenomena are forced by safety factor around the major rational number of 1/2, 1/2 and 2/3. The line averaged electron density

pumps out and sustains low level of order of $10^{19}m^{-3}$. In this discharge, ion is heated explosively together with the plasma fluctuations.

3.2.2 *ATRAS RFP Experiment*

ATRAS Device (Nihon Univ.)

ATRAS is a RFP machine with major and minor radii of R=0.5m and a=0.1m respectively. Thirty two stainless-steel limiters are included into the vacuum vessel, and limit the plasma minor radius of 0.09m. The vacuum vessel, which is made of stainless-steel below with the thickness of 0.4mm, is covered by Aluminum double shell of 100mm thickness. The characteristic of ATRAS device is that it has two independent Ohmic heating (OH) circuits. former regards as the 'OH-1', that is for the standard RFP plasma and the latter is 'OH-2', that is for the additional rising up of plasma currents.

Diagnostic Systems

Top view of ATRAS's diagnostic system is illustrated in Fig.3.8. Plasma current and loop voltage are measured by Rogowski coil and toroidal flux loops around the vacuum vessel respectively. Fore poloidal flux loops are wounding poloidally at the angle of 90 degree the intervals around the vacuum vessel to measure the toroidal flux and averaged toroidal magnetic field. Magnetic probes, which measure the poloidal and radial magnetic field, are installed between vacuum vessel and Aluminum double shell. The MHD fluctuations, plasma position and toroidal and poloidal mode numbers can be estimated. One magnetic probe located outside of shell measures the toroidal magnetic field to estimate the reversal parameter F(See section 3.2.3). Electron temperature is measured by Surface Briar Diode(SBD) and ion temperature is measured by visible light spectrometer. CO_2 interferometer will be installed for measurement the line-averaged electron density $\overline{n_e}$.

Additional Loop Voltage for the Experiments of Induced Toroidal Electric Field

The characteristic of ATRAS power supply system for Ohmic heating is two independent poloidal coil circuit [61]. The quarter period of OH-1 coil is 1.5msec and maximum volt second is 0.21V.sec. The another is Ohmic-2 circuit(OH-2), which induces the additional loop voltage during RFP discharge with the time constant of 0.55msec. That value of rising time of OH-2 circuit can be changed by variable connection methods of OH-2 coils. Figure 3.9 shows the time evolution of loop voltage with and without OH-2 circuit. This experiment regards as 'E_t pulsed Experimental'.

Typical ATRAS RFP Discharge

ATRAS RFP experiment has been carried out in the range of $I_p < 60kA$ using only OH-1 circuit. Figure 3.10 shows the typical RFP discharge waveforms. Plasma current I_p, one turn voltage V_{loop}, averaged toroidal magnetic field $< B_t >$, toroidal magnetic field at the plasma surface B_{zw}, pinch parameter θ, reversal parameter F and four toroidal flux are shown. The RFP configuration is obtained from about 0.2[msec], where plasma current reaches its maximum value at about 1.0[msec]. Plasma duration time is about 2.5[ms]. In normal operation, the value of θ lies at high value of ~ 2.0 with field reversal parameter of about ~ -0.5.

In present interesting topics of RFP, the toroidal rotation of asymmetric toroidal magnetic flux perturbations are observed [62, 63, 64]. In ATRAS experiment, such rotation of toroidal flux perturbations are investigated, accompanied with the enhancement of MHD mode as shown in Fig.3.11. We can see the strong correlation between its rotation and the enhancement of the m=1 kink mode. The velocity of its rotation become more slower as linear function of time.

3.2.3 *Experimental Data along $F - \theta$ Curve*

The theoretical curve of F and θ is illustrated in Fig.2.3. This is so-called '$F - \theta$ diagram', and it shows an important way of representing the behavior of pinch distributions. The operational range of ULQ discharge is $0 < F < 1$ ($0 < \theta < 1.2$). Figure 3.12 shows a theoretical $F - \theta$ curve and experimental data points on ULQ discharge. The experiment data almost agree with the theoretical curve. The slippage between theory and experiment results is caused by assumption of the pressure-less plasma with a finite plasma current density at the wall, in contrast to experiment in which the plasma pressure is typically $10\% \sim 30\%$ of the magnetic pressure and the current density approaches to zero at the wall [66, 67, 68].

In RFP configuration the characteristic is the reversal toroidal magnetic field on the outside of plasma. The experimental data of RFP discharge are also almost agreement on the theoretical $F - \theta$ diagram as shown in Fig.3.13. The operational range of RFP discharge is $F < 0$ ($1.2 < \theta$).

3.3 *Typical Waveform with Induced Pulse Electric field*

3.3.1 *Positive E_p Pulsed Experiment in REPUTE-1*

Time evolution of plasma parameters, in the case when toroidal magnetic field is rapidly decreased during ULQ discharge, is shown in Fig.3.14. The figure shows averaged toroidal magnetic field $< B_t >$, toroidal current I_p, one turn voltage V_{loop}, safety factor at the wall q_a, the center chord averaged electron density $\overline{n_e}$, pinch parameter θ, reversal parameter F, poloidal magnetic fluctuation $\mid \widetilde{B_p} \mid_{rms}$ and effective resistivity η. The standard ULQ configuration with $q_a \sim 0.4$ is initially set up and the toroidal magnetic field is decreased quickly with a time constant of $\sim 0.3ms$. Synchronized to the decrease of the toroidal magnetic field, of course, the poloidal plasma current increases, the increase of the toroidal plasma current is observed, accompanied with the decrease of loop voltage.

This experimental results indicate that the toroidal current density j_t, is con-

verted by poloidal current density j_p, induced by a fast decrease of the toroidal magnetic field and it is experimental confirmation of half cycle of closed circle of dynamo effect. ($B_p \rightarrow B_t$)

Figure 3.15 shows the plasma responses to a varied change ratio of toroidal magnetic field. We can see that the change rate of plasma parameter become lager, as the change ratio of the toroidal magnetic field.

Thus the effective η, which is estimated by plasma current and loop voltage, is decreased. This improvement of plasma performance can be accounted for the application of the poloidal electric field. It is inferred that a poloidal component of dynamo electric field, which is strong coupled with plasma fluctuations, is partly replaced with the induced poloidal electric field, because the direction of this induced field is the same with that of dynamo electric field. We can see although the magnetic field became weak, the magnetic fluctuations do not enhance in this phase. This result is not explained by the empirical scaling in ULQ plasmas the resistance anomaly becomes large, as the toroidal magnetic field become weak [60](See section 3.1.4).

3.3.2 *Negative E_p Pulsed Experiment in REPUTE-1*

During ULQ discharge, the toroidal magnetic field is rapidly increased. Figure 3.16 shows the averaged toroidal magnetic field $< B_t >$, toroidal current I_p, one turn voltage V_{loop}, safety factor at the wall q_a, the center chord averaged electron density $\overline{n_e}$, pinch parameter θ, reversal parameter F, poloidal magnetic fluctuation $\mid \widetilde{B_p} \mid_{rms}$ and effective resistivity η. The standard ULQ configuration with $q_a \sim 0.2$ is initially set up and the toroidal magnetic field is increased quickly with a time constant of $\sim 0.3ms$. During the increasing phase of toroidal magnetic field, increase of the loop voltage is observed accompanied with enhancement of plasma fluctuations. While, plasma current is maintained almost constant and effective resistivity is increased in this phase. This behavior also can be accounted for the induction of the poloidal electric field, which direction is the opposite with that of dynamo

electric field.

After the increase of toroidal magnetic field($t = 1.1 \sim 3.0ms$), in which phase the externally induced poloidal electric field is almost zero, plasma current begins to increase slowly, accompanied with the decrease of the loop voltage. The maximum value of increased plasma current is limited by large MHD activity. These behaviors will be discussed in section 3.7.

3.3.3 *E_t Pulsed Experimental in ATRAS*

Time evolution of plasma parameters, in the case when additional loop voltage is rapidly applied during the RFP discharge is shown in Fig.3.17. Time evolutions of toroidal plasma current I_p, one turn voltage V_{loop}, averaged toroidal magnetic field $< B_t >$, toroidal magnetic field at the plasma surface B_{zw}, pinch parameter θ, reversal parameter F and four toroidal flux are shown. The standard RFP configuration with pinch parameter, $\theta \sim 1.5$ and reversal parameter, $F \sim -0.3$ is initially set up and additional toroidal loop voltage is applied with a time constant of $\sim 0.55ms$. Synchronized to the application of the additional loop voltage, of course, I_p increases, the increase of the $< B_t >$ is observed. This result indicates poloidal current density is converted by induced toroidal electric field. In this phase, pinch parameter θ, and reversal parameter F, are kept almost constant. It is inferred that the toroidal and poloidal components is strong coupled through the dynamo effect.

This experimental result indicates the poloidal current density j_p, is generated by toroidal current density j_t, induced by the application of the additional toroidal loop voltage and it is experimental confirmation of another half cycle of closed circle of dynamo effect ($B_p \rightarrow B_t$). Figure 3.18 shows the responses of toroidal flux to a varied change of additional toroidal loop voltage. We can see that the change of toroidal flux becomes larger, as the change of the toroidal plasma current I_p is large, hence pinch parameter, θ and reversal parameter F is maintained almost constant.

3.4 *Trajectory on F-θ Diagram*

3.4.1 *Positive E_p Pulsed Experiment in REPUTE-1*

In this section, we consider the variations of the pinch parameter θ and reversal parameter F, when the induced toroidal and poloidal pulse electric fields are applied.

Figure 3.19 shows the trajectory on the $F - \theta$ diagram, in the case of positive E_p pulsed experiment. Synchronized to the decrease of the toroidal magnetic field, F is decreased quickly with constant value of θ, and comes near the BFM. After then its characteristic is returned quickly and moves on the experimental scaling of the $F - \theta$ curve. We can see that when toroidal magnetic field is decreased, the ULQ plasma changes their characteristic following BFM.

Generally when RFP configuration is formed, the toroidal magnetic field is reversed as the increase of plasma current. This behavior indicates the positive driving of θ makes decrease the F value and F value become negative value in RFP region. This experiment result shows the opposite process as compared with standard RFP formation process. We reduce the F value and its response is increase of the θ value. This is a experimental verification that ULQ plasma is a also member of the Taylor state, similar to RFP configuration.

3.4.2 *Negative E_p Pulsed Experiment in REPUTE-1*

Figure 3.20 shows the trajectory on the $F - \theta$ diagram, in the case of negative E_p pulsed experiment. We can see that when toroidal magnetic field is increased, the plasma characteristic also changes following BFM.

We describe in full the transient phase in these experiments. Synchronized to increase of the toroidal magnetic field, in this phase loop voltage slight increases, accompanied with enhancement of plasma fluctuations and plasma current is maintained almost constant value. The plasma characteristic tends to be shift slightly on the $F - \theta$ curve toward the high F region with constant θ value. This reason is considered to be the effect of peak of the plasma channel due to the magnetic

compression. After that, plasma characteristic returns on the $F-\theta$ diagram quickly and reaches the minimum value of θ. Finally in the phase of increase of the toroidal plasma current, θ increases due to the increase of the plasma current and F value is slight decreased, thus, plasma characteristic changes along the BFM.

3.4.3 *E_t Pulsed Experimental in ATRAS*

Figure 3.21 shows the trajectory on the $F-\theta$ diagram, in the case of E_t pulsed experiment. We can see that the pinch parameter θ and reversal parameter F are maintained almost constant during this phase, although the plasma current is increased, due to the additional loop voltage. This result indicates that after the RFP configuration is setup, although the magnitude of magnetic or electric fields is changed, the distribution of RFP configuration is not changed.

3.5 *Trajectory on η-B_t Scaling*

3.5.1 *Positive E_p Pulsed Experiment in REPUTE-1*

Figure 3.22 shows the trajectory on the experimental scaling of the plasma resistivity η^* as a function of the toroidal magnetic field, in the case of positive E_p pulsed experiment. The standard ULQ configuration with effective plasma resistivity $\eta^* \sim 40\mu\Omega m$ is set up and maintained until 1.5msec, and toroidal magnetic field is decreased quickly with a time constant of $\sim 0.3ms$. Synchronized to decrease of the toroidal magnetic field, decrease of the η^* is observed. This result is not explained by the empirical scaling, ULQ plasmas the resistance anomaly becomes large, as the toroidal magnetic field becomes weak [60](See section 3.1.4). This reason is considered to be that a poloidal component of plasma current is partly supported by induced pulsed positive electric field, because the direction of that electric field is the same with that of dynamo electric field, and f and θ values come near the the theoretical $F-\theta$ diagram.

3.5.2 *Negative E_p Pulsed Experiment in REPUTE-1*

Figure 3.23 shows the trajectory on the experimental scaling of the plasma resistivity η^* as a function of the toroidal magnetic field, in the case of negative E_p pulsed experiment. The standard ULQ configuration with effective plasma resistivity $\eta^* \sim 50\mu\Omega m$ is set up and maintained until 1.0ms, and toroidal magnetic field is increased quickly with a time constant of $\sim 0.3ms$. Synchronized to increase of the toroidal magnetic field, increase of the η^* is observed. This result is can also be accounted for dynamo electric field, similar to the positive E_p pulsed experiment.

After the increase of toroidal magnetic field, in this phase toroidal plasma current increases slowly, accompanied with decrease of the loop voltage, the remarkable decrease of η^* is observed. This characteristic will be discussed in section 3.6. After the phase of improvement of plasma confinement, the effective plasma resistivity returns on the standard ULQ plasmas.

These results support that dynamo electric field plays an essential role in the deterioration of the plasma performance and the additional poloidal electric field strong influences the plasma performance.

3.6 *Variations of Internal Structure in the Transient Phase*

3.6.1 *Positive E_p Pulsed Experiment in REPUTE-1*

To investigate of the variations of the internal magnetic field structures and profiles in the transient phase, the array of the magnetic probe, covered with SUS pipe of 0.5mm thickness, is inserted into the plasma, as shown in Fig.3.5. The toroidal and poloidal magnetic field profiles, in the case of positive E_p experiment are shown in Fig.3.24. The toroidal magnetic field is decreased at the time of 1.5msec rapidly. We can see that the center of toroidal magnetic field is enhanced due to the dynamo effect. The profile of the toroidal and poloidal current densities are estimated from the profile of magnetic fields as follows,

Toroidal Current Density $j_t = -\frac{1}{\mu_0 r}\frac{\partial}{\partial r}(rB_p)$,

Poloidal Current Density $j_p = \frac{1}{\mu_0 R}\frac{\partial}{\partial r}(RB_r)$,

where $R = R_0 + r$, R_0 is a major radius, are shown in Fig.3.25. Synchronized to decrease of the toroidal magnetic field, the remarkable increase of the poloidal current density is observed. This result is accounted for the induced positive poloidal electric field. We can see the enhancement of both current densities although decrease of the toroidal magnetic field.

The time evolution of the safety factor profile is shown in Fig.3.26. The configuration with pitch minimum is kept during the decreasing phase of the toroidal magnetic field. The change of safety factor at the plasma surface is relatively continuous function of time. While around the plasma center, the response of the safety factor seems to be stepwise. The safety factor around the plasma center does not change so much during $t = 1.47 \sim 1.92ms$, and decreases quickly at $t = 1.95msec$. The stepwise decrease of the plasma current has also been observed in constraint field ULQ experiments when the safety factor pass through the rational surface.

3.6.2 *Negative E_p Pulsed Experiment in REPUTE-1*

The toroidal and poloidal magnetic field profiles in the case of negative E_p pulsed experiment are shown in Fig.3.27. The toroidal magnetic field is increased at the time of 1.0msec rapidly. We can also see that the center of toroidal magnetic field is enhanced due to the dynamo effect. The profiles of the toroidal and poloidal current densities estimate from the profiles of magnetic fields, are shown in Fig.3.28. Synchronized to the increase of toroidal magnetic field, the remarkable decrease of the poloidal current density in the edge region is observed. This result is also accounted for the induced negative poloidal electric field. After the transient phase, the poloidal current density profile is returned to the standard ULQ profile at the outside of the plasma and profiles of toroidal and poloidal current densities are sustained almost same ones and increased slowly. This results indicate the force free field is strong and magnetic field structure is maintained.

While the time evolution of safety factor profile as a function of minor radius in the case when toroidal magnetic field is increased, is shown in Fig.3.29. In the transient phase, the safety factor at the plasma surface, increases with a relatively continuous function of time. On the other hand, the safety factor around the plasma center does not change so much during $t = 1.25 \sim 1.35ms$ and after then it stepwise increases until end of the increase of the toroidal magnetic field. In such a transient phase, the different characteristic from standard ULQ configuration is as follows, one is the safety factor profile is $dq_{(r)}/dr > 0$ in the bulk of plasma region, and other is the safety factor passes through the many rational surface.

Just after increase of the toroidal magnetic field, plasma current increased slowly. In this phase, profile of safety factor is returned to similar standard ULQ configuration ($dq_{(r)}/dt < 0$ in the bulk of plasma region) and decreases until the large rational surface. After then the enhancements of plasma resistivity and plasma fluctuation are observed.

Other plasma parameters are estimated from toroidal and poloidal magnetic field profiles as follows;

Plasma major radius	R_0,	
Induced poloidal electric field	E_{ind}	$= -\frac{1}{r}\int_0^r (r\frac{\partial B_t}{\partial t})dr$,
Plasma minor radius	a^*,	
Internal inductance	l_i	$= \frac{2}{a^2 B_{p(a)}{}^2}\int_0^a B_{p(r)}{}^2 r dr$,
Plasma resistivity	η^*	$= \frac{a}{2R}\left[\frac{V_{loop}}{I_p} - \frac{1}{I_p}\frac{d}{dt}(L_p I_p)\right]$,
	L_p	$= \mu_0 R_0 \left(ln\frac{R_0}{a} + \frac{l_i}{2} - 2\right)$,

Figure 3.30 shows the time evolution of averaged toroidal magnetic field $< B_t >$, plasma current I_p, loop voltage V_{loop}, safety factor at the wall q_a, effective plasma resistivity η^*, shift of major radius ΔX, plasma minor radius a^*, internal inductance l_i and induced poloidal electric field E_{ind}. These behavior can be distinguished into three phases as follows:

- Negative E_p induced phase($t = 1.0 \sim 1.3ms$).
  - Loop voltage V_{loop}, is increased slightly and plasma current I_p, is maintained almost constant.
  - Synchronized to increase of the toroidal magnetic field, effective plasma resistivity η^*, is enhanced immediately.
  - Shrinkage of plasma minor radius a^*, is observed.
  - Internal inductance l_i, is kept almost constant ~ 0.7.
  - Induced negative poloidal electric field is impressed $\sim 25V/m$, which direction is opposite to dynamo electric field as shown in Fig.3.31.
- After the phase of induced negative electric field($t = 1.3 \sim 2.2ms$).
  - Toroidal plasma current I_p, is increased slowly, accompanied with decrease of loop voltage V_{loop}
  - Effective plasma resistivity η^*, is remarkable decreased.
  - Shrinkage of the plasma column a^*, is returned toward initial minor radius.
  - Internal inductance l_i, is kept almost constant ~ 0.7.
  - Induced negative poloidal electric field decreases almost zero due to the condition of $dB_t/dt \sim 0$.
- After the phase when increase of toroidal plasma current reaches its maximum value($t = 2.2ms \sim$).
  - loop voltage V_{loop}, increases slightly and plasma fluctuation is enhanced.
  - Effective plasma resistivity η^*, is reset toward its value of standard ULQ plasma.

3.7 *Behavior of After Transient Phase*

3.7.1 *Positive E_p Pulsed Experiment in REPUTE-1*

After the decrease of the toroidal magnetic field, as shown in Fig.3.14, plasma configuration is returned to standard ULQ plasma, in this phase toroidal magnetic field is low, and induced poloidal electric field is almost zero. In these experiments, magnetic field lines are twisted more than initial ULQ configuration. When the toroidal magnetic field is reduced almost zero or negative fields plasma discharge is terminated immediately, accompanied with enhancement of plasma fluctuation.

3.7.2 *Negative E_p Pulsed Experiment in REPUTE-1*

Just after the toroidal magnetic field is increased to its maximum value, the plasma current begins to increase slowly, accompanied with the decrease of the loop voltage. In these experiment magnetic field lines are relaxed its twist more than initial ULQ configuration. After then the magnetic field line tends to twist again spontaneously due to the increase of plasma current.

During the increasing phase of the toroidal magnetic field, the safety factor at the wall increases, and it becomes the maximum value $q_{a.max}$. Subsequently, the safety factor begins to decrease, due to the increase of the plasma current, and it becomes the minimum settled value $q_{a.settle}$. Figure 3.32 shows the correlation between $q_{a.max}$ and $q_{a.settle}$. We can see that the value of $q_{a.settle}$ are spreading around rational number of 1/3, 1/2 and 2/3. This result indicates that the maximum value of the plasma current is limited by large MHD activity.

After the plasma current is limited by MHD activity, the plasma fluctuations enhances, as shown in Fig.3.33. This result is considered to be caused by the safety factor partly touches on the rational surface in this phase. For example the time evolution of plasma current I_p, and loop voltage V_{loop}, safety factor at the wall q_a and effective plasma resistivity η^* in the case when plasma current increases against $q_a = 1/2$ rational surface are shown in Fig.3.34(a), and time behavior of its safety

factor profile is shown in Fig.3.34(b). In Fig.3.34(a), increase of plasma current is stopped at the $q_a = 1/2$ temporary, resulting in the enhancement of effective plasma resistivity η^*, and begins to increase again, accompanied with the decrease of the effective plasma resistivity η^*. Figure 3.34(b) shows the time evolution of safety factor at this discharge.

3.7.3 *E_t Pulsed Experimental in ATRAS*

In ATRAS RFP and other RFP experiments the rotation of toroidal flux perturbations is observed as correlation with MHD mode as shown in Fig.3.11. Figure 3.35 shows the behavior of toroidal flux perturbation when the additional loop voltage is applied during RFP plasma. We can see that there is also strong correlation between its rotation and the enhancement of the m=1 kink mode and the velocity of their rotation become more slower as linear function of time, before application of additional loop voltage. While, after the induction of additional loop voltage, the velocity of rotation of toroidal flux perturbations tends to be returned to original one.

3.8 *Discussion and Conclusion*

In RFP and ULQ plasmas there exists the poloidal electric field, which is driven by exciting plasma fluctuations through the dynamo effect (turbulent electric field). To investigate such dynamo effects on RFP and ULQ plasmas, toroidal and poloidal pulsed electric fields are induced on standard low q discharges. The pulsed poloidal electric field is induced by a fast changing of the toroidal magnetic field, and pulsed toroidal electric field is applied by additional increase of loop voltage.

At first, in the case when the toroidal magnetic field rapidly decreases during the ULQ discharge, the direction of externally-induced poloidal magnetic field is the same as that of dynamo electric field. Synchronized to the decrease of the toroidal magnetic field, also the poloidal plasma current is increased, the increase of the toroidal plasma current is observed, accompanied with the decrease of loop

voltage. These results indicate that poloidal magnetic field is converted by induced toroidal magnetic field, and this behavior is a experimental verification of the half part of closed circle of dynamo effect ($B_t \Rightarrow B_p$). Figure 3.36 shows the trajectory on the $F-\theta$ diagram in transient phase. In positive E_p pulsed experiment, plasma characteristic seems to be come near BFM and after then which returns near the experimental $F-\theta$ curve immediately. This result indicates that configuration of force free field is strong, and when its structure is changed by the external forces, plasma characteristic is returned to original state immediately. In this experiment, the effective η is decreased. The improvement of plasma performance can be accounted for the poloidal electric field. It is inferred that a poloidal component of dynamo electric field, which is strong coupled with plasma fluctuations, is partly replaced with the induced poloidal electric field. Figure 3.37 shows the reduction rate of resistance as a function of the changing rate of the toroidal magnetic field, where the negative value of dB/dt corresponds to the positive E_p pulsed experiments. The decrease of the resistance anomaly becomes larger, as the changing rate of the toroidal magnetic field increases. Figure 3.38 shows the changing rate of magnetic fluctuation levels as a function of the changing rate of the toroidal magnetic field, where the negative value of dB/dt corresponds to the positive E_p pulsed experiments. We can see that the changing rate of magnetic fluctuation is slight decreased or almost constant although the toroidal magnetic field becomes low magnitude. This reason is accounted that F and θ values come near the theoretical BFM. When the change of F value is enough to large, in this state F slips out in the lower region of BFM, resulting in the enhancement of plasma fluctuations.

At the second experiments, a fast rising of the toroidal magnetic field is applied for ULQ plasma, where the direction of the induced poloidal electric field is opposite to that of dynamo electric field. During the increasing phase of toroidal magnetic field, increase of the loop voltage is observed, accompanied with enhancement of plasma fluctuations. While, plasma current is maintained almost constant and effective resistivity is increased in this phase. The changing rate of magnetic

fluctuation levels as a function of the changing rate of the toroidal magnetic field, is depicted in Fig.3.38, and the rate of resistance as a function of the changing rate of the toroidal magnetic field is depicted in Fig.3.37, where the positive value of dB/dt corresponds to the positive E_p pulsed experiments. This behavior also can be accounted for the poloidal electric field, similar to 'Positive E_p pulse experiment', that direction is the opposite to that of dynamo electric field. Figure 3.36 depicts the trajectory on the $F-\theta$ diagram in transient phase in the case of negative E_p pulsed experiments. Just after increase of toroidal magnetic field, plasma characteristic is also slipped out of BFM and that returns near the theoretical model immediately. These results also show that condition of force free field is strong, and when it structure is changed by external forces, plasma characteristic is returned to original state immediately.

At the third experiments, the toroidal electric field is applied during RFP discharge instantaneously. Synchronized to the application of the additional toroidal loop voltage, of course, the toroidal plasma current is increased, the increase of the averaged toroidal magnetic field is observed. In this phase, pinch parameter θ and reversal parameter F are kept almost constant. These experimental results indicate, in contrast to the E_p pulsed experiments, the poloidal current density j_p, is converted by toroidal current density j_t and it is experimental confirmation of another half cycle of closed circle of dynamo activity.

In these experiments, we can see the closed process of generation. The toroidal magnetic field is converted by the induced poloidal magnetic field, and the generation of poloidal magnetic field is converted by the toroidal magnetic field through the dynamo effect in force free field.

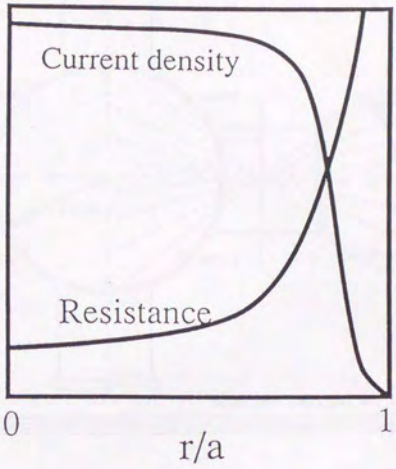

Figure 3.1: Schematic drawing of current density and plasma resistivity profiles.

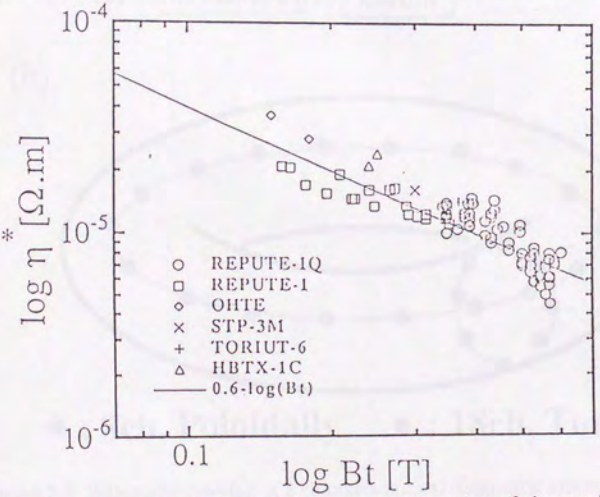

Figure 3.2: Scaling of effective resistivity η^*, as a function of the toroidal magnetic field B_t.

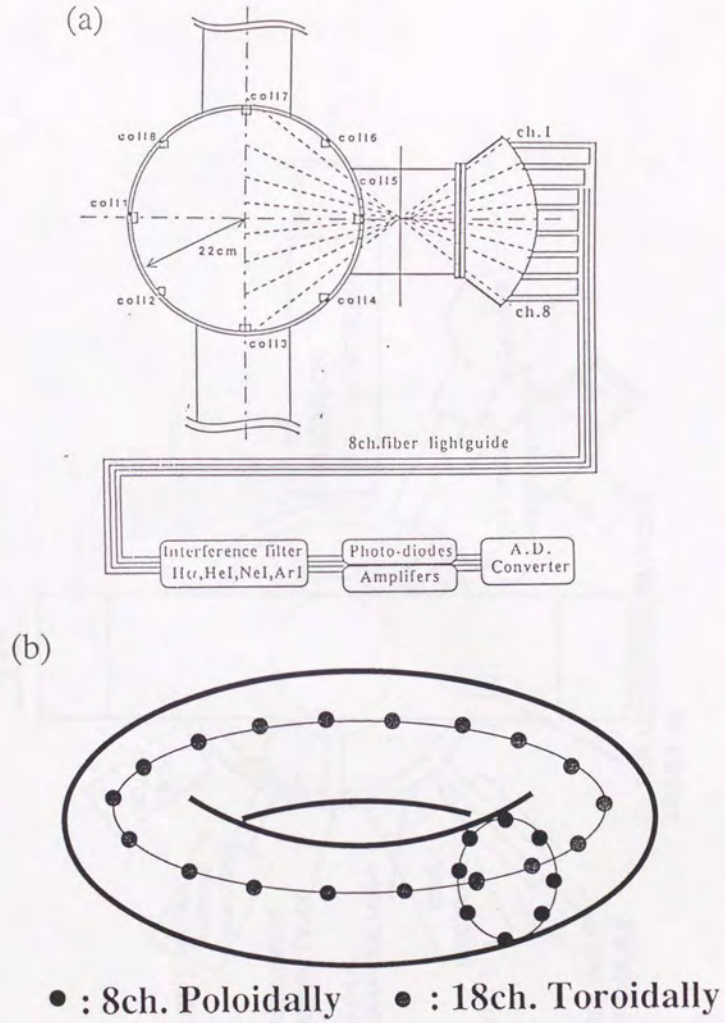

Figure 3.3: Schematic drawing of 8 channels optical diagnostic system(a) and layout of edge toroidal and poloidal magnetic probes arraignments(b).

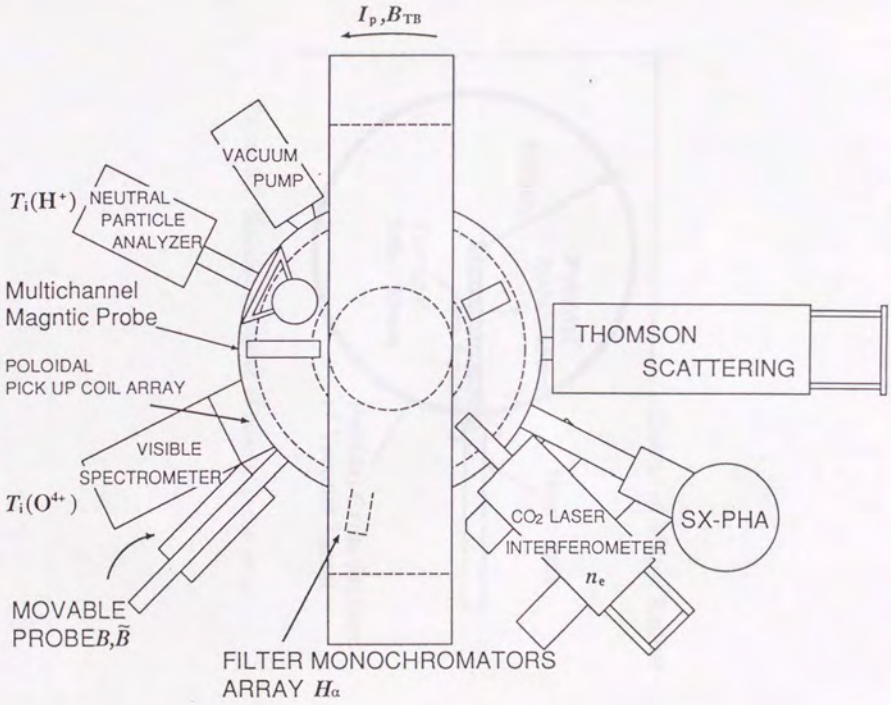

Figure 3.4: The layout of diagnostic system of REPUTE-1.

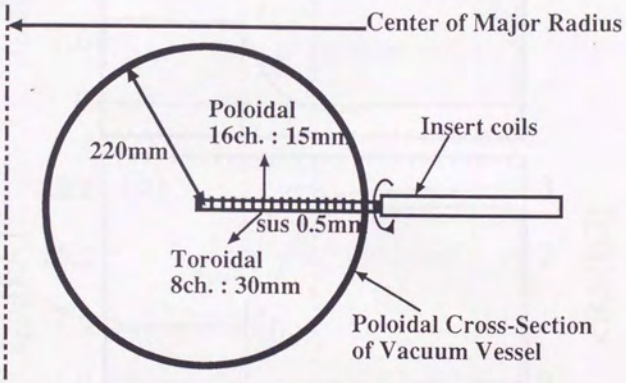

Figure 3.5: Schematic drawing of internal probe array.

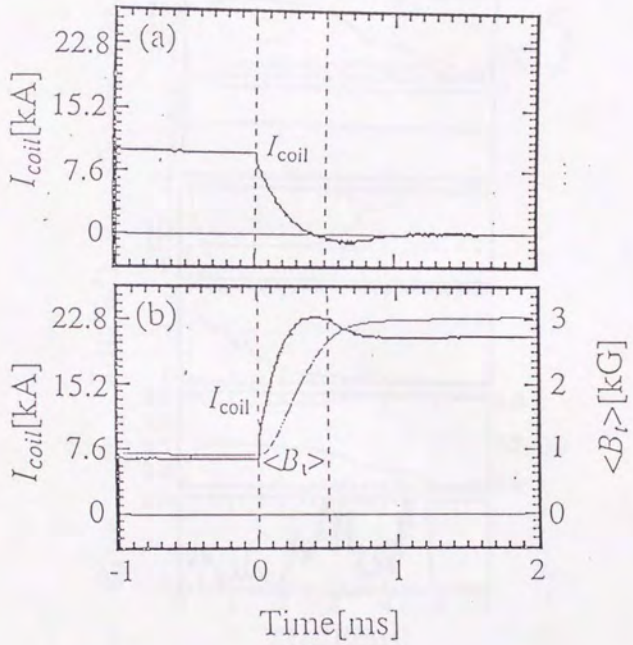

Figure 3.6: (a)Time evolution of toroidal coil current for the case of positive E_p experiment. (b)Time evolution of toroidal coil current and averaged toroidal magnetic field for the case of negative E_p experiment.

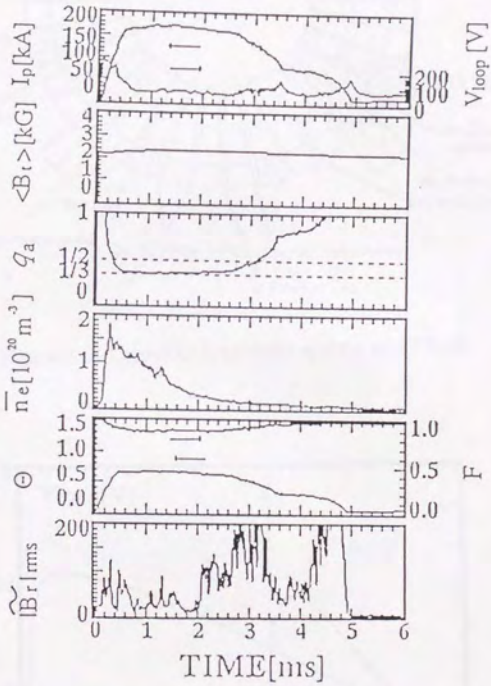

Figure 3.7: Typical ULQ waveform.

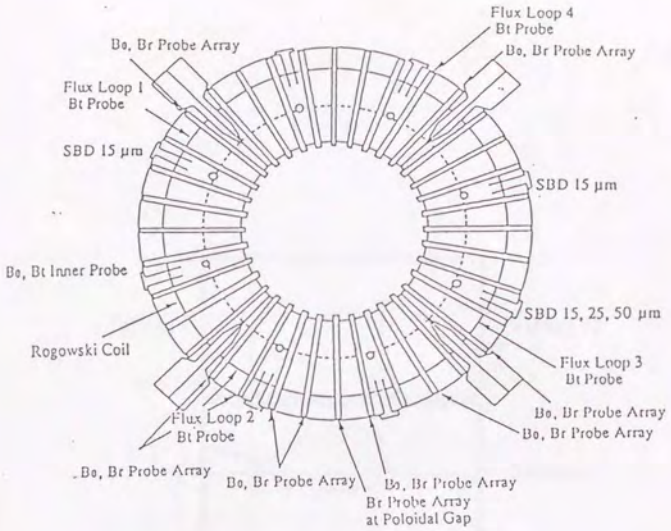

Figure 3.8: Layout of diagnostic system of ATRAS.

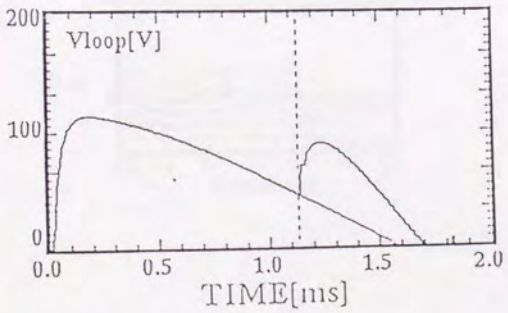

Figure 3.9: Time evolution of loop voltage with and without OH-2 circuit.

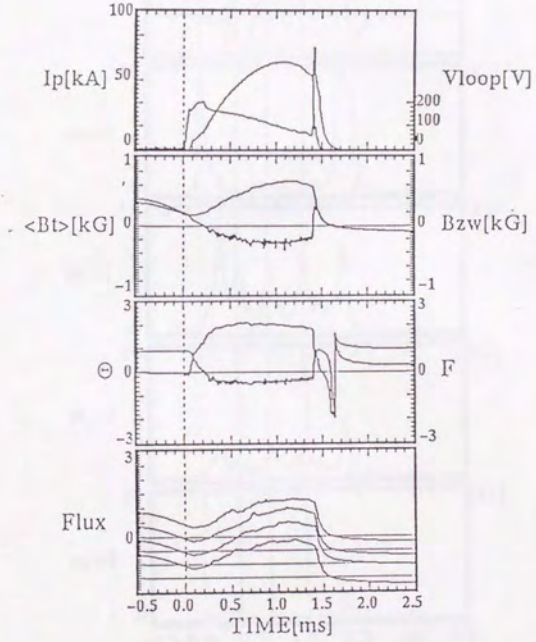

Figure 3.10: Typical RFP waveform.

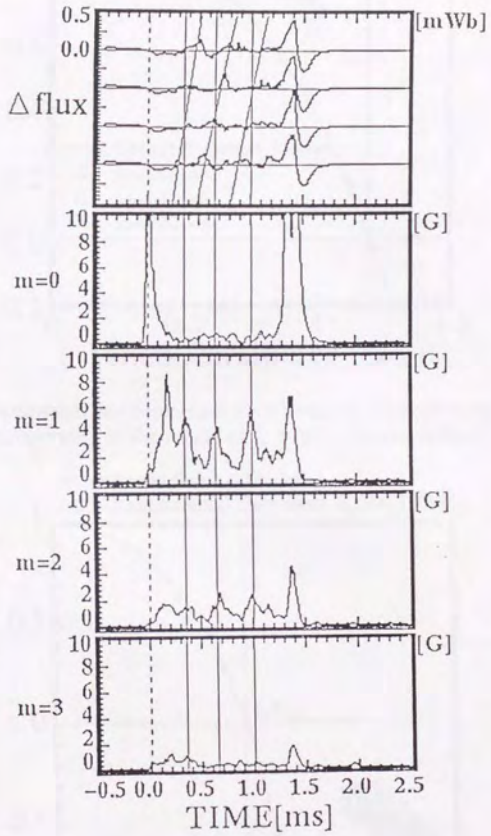

Figure 3.11: Toroidal flux perturbation at four different toroidal location and MHD mode activity. The diagonal line traces the motion of a flux perturbation and peak of m=1 mode.

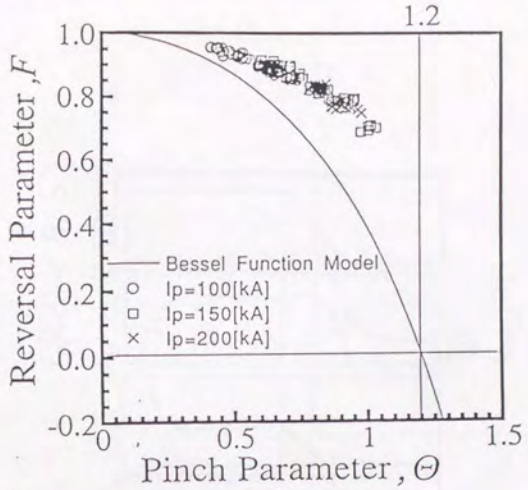

Figure 3.12: Experimental and theoretical $F-\theta$ diagram. The point from REPUTE-1 ULQ discharges operated in the region of $I_p = 100, 150$ *and* $200[kA]$.

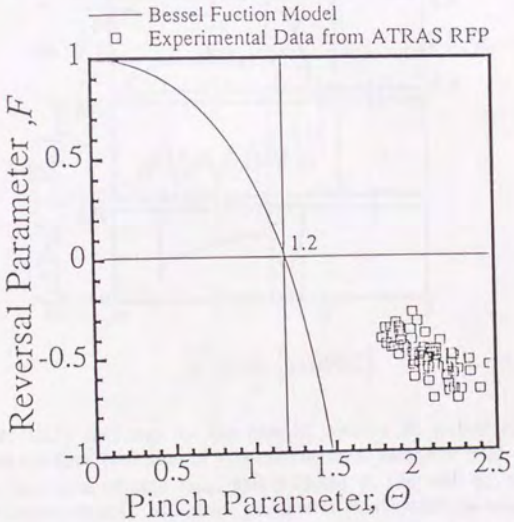

Figure 3.13: Experimental and theoretical $F-\theta$ diagram. The point from ATRAS RFP discharges.

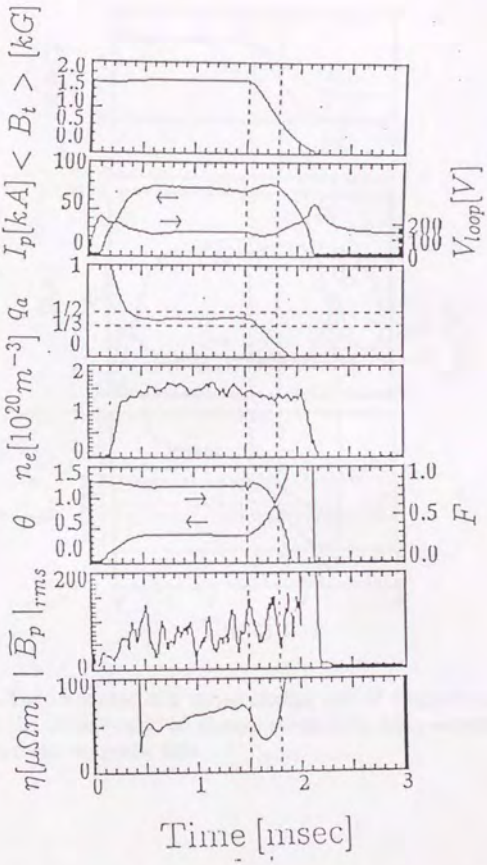

Figure 3.14: ULQ discharge for the case of positive E_p pulsed experiment. The figure shows the time evolution of averaged toroidal magnetic field $< B_t >$, toroidal current I_p, one turn voltage V_{loop}, safety factor at the wall q_a, the center chord averaged electron density $\overline{n_e}$, pinch parameter θ, reversal parameter F, poloidal magnetic fluctuation $|\widetilde{B}_p|_{rms}$ and effective resistivity η.

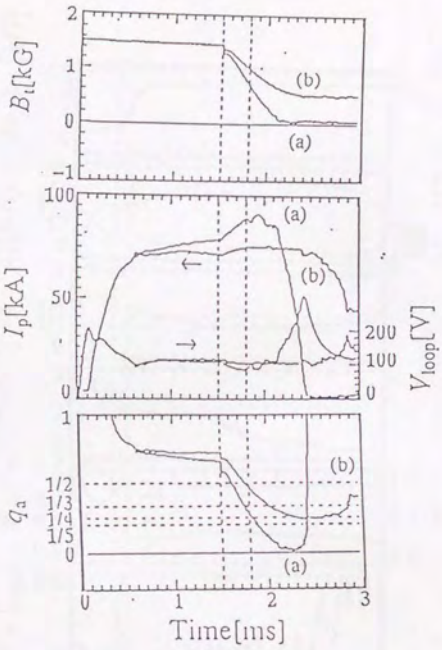

Figure 3.15: The responses to a varied change rate of toroidal magnetic field. We can see that the change ratio of plasma parameters become lager, as the change ratio of the toroidal magnetic field.

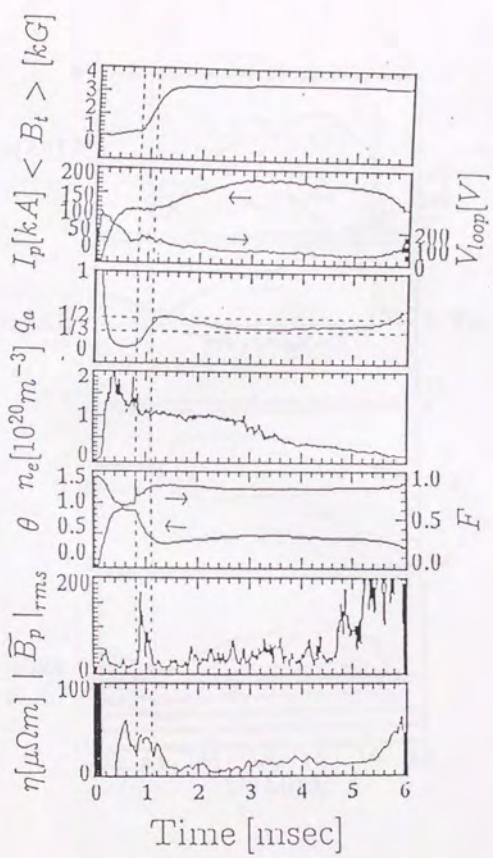

Figure 3.16: ULQ discharge for the case of negative E_p pulsed experiment. The figure shows the time evolution of averaged toroidal magnetic field $< B_t >$, toroidal current I_p, one turn voltage V_{loop}, safety factor at the wall q_a, the center chord averaged electron density $\overline{n_e}$, pinch parameter θ, reversal parameter F, poloidal magnetic fluctuation $| \widetilde{B}_p |_{rms}$ and effective resistivity η.

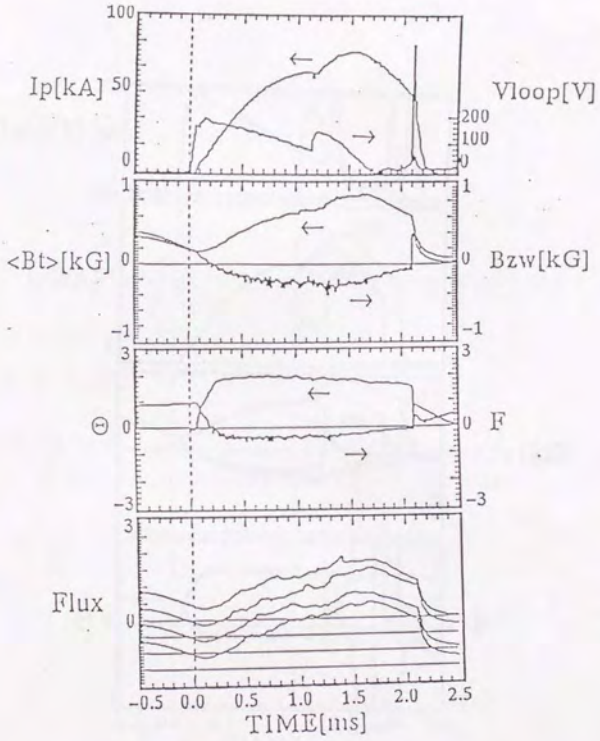

Figure 3.17: RFP discharge for the case of E_t pulsed experiment. The figure shows the time evolutions of toroidal plasma current I_p, one turn voltage V_{loop}, averaged toroidal magnetic field $< B_t >$, toroidal magnetic field at the plasma surface B_{zw}, pinch parameter θ, reversal parameter F and four toroidal flux $Flux$.

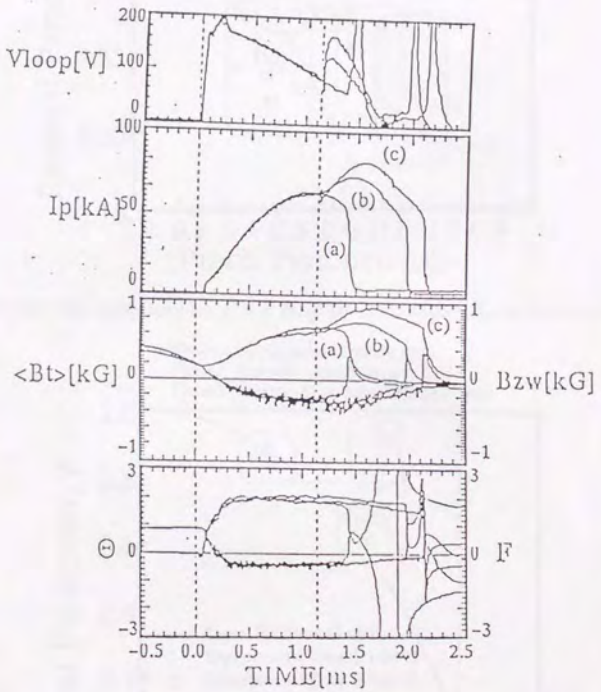

Figure 3.18: The responses to a different change rate of additional loop voltage. We can see that, in these experiments, the changing of averaged toroidal magnetic field $< B_t >$, becomes larger, as the change of the toroidal plasma current I_p is large and toroidal magnetic field at the plasma surface is sustained almost constant. Hence pinch parameter θ, and reversal parameter F, is maintained almost constant.

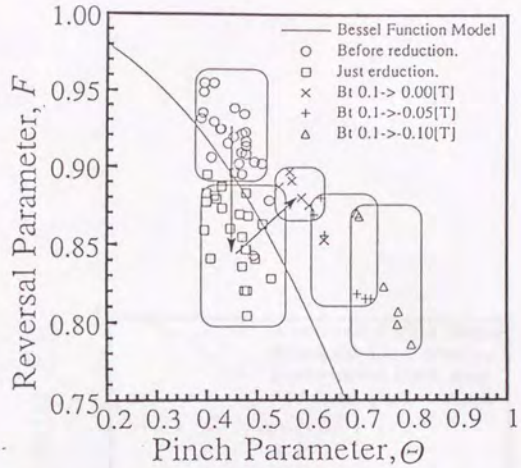

Figure 3.19: The trajectory on $F - \theta$ diagram on positive E_p pulsed experiments.

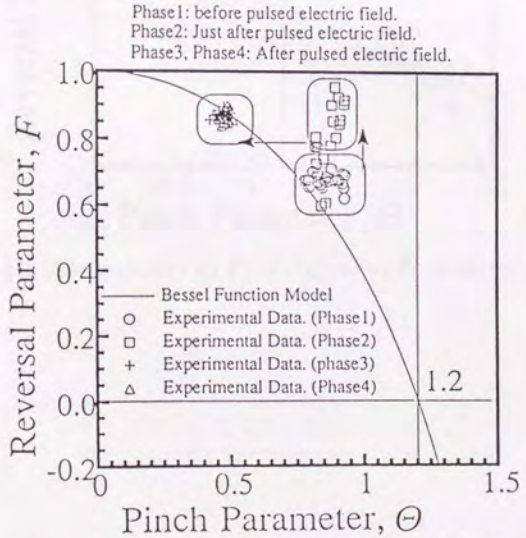

Figure 3.20: The trajectory on $F - \theta$ diagram on negative E_p pulsed experiments.

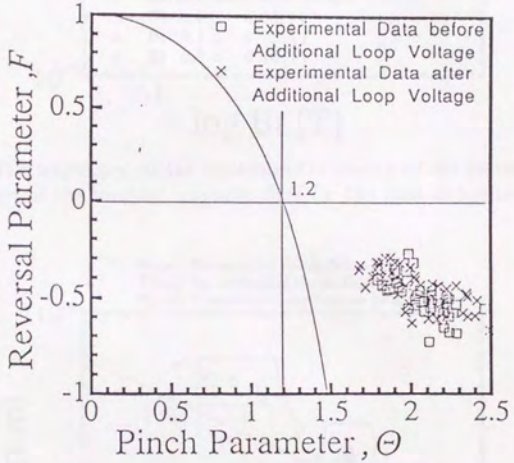

Figure 3.21: The trajectory on $F - \theta$ diagram on E_t pulsed experiments.

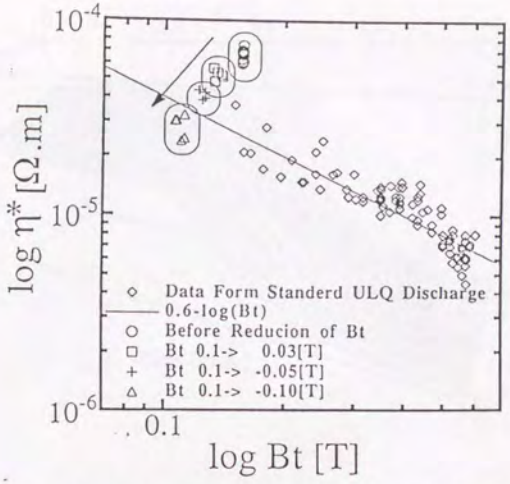

Figure 3.22: The trajectory on the experimental scaling of the plasma resistivity η^* as a function of the toroidal magnetic field for the case of positive E_p pulsed experiment.

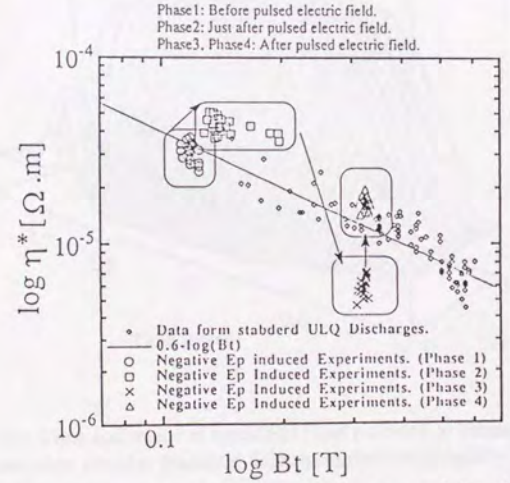

Figure 3.23: The trajectory on the experimental scaling of the plasma resistivity η^* as a function of the toroidal magnetic field for the case of negative E_p pulsed experiment.

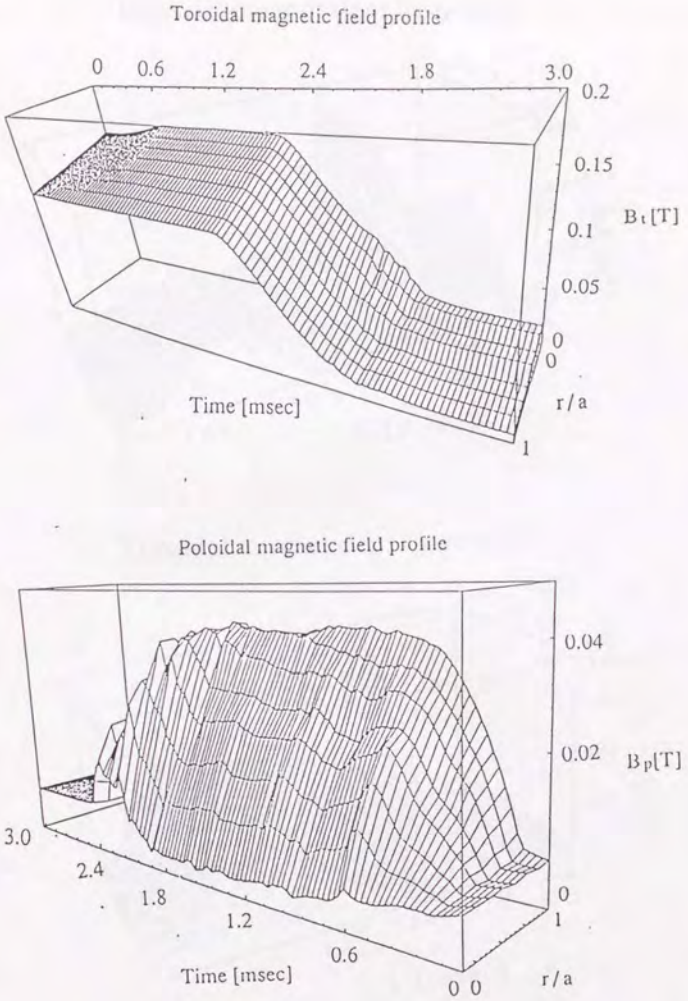

Figure 3.24: Time evolutions of toroidal(a) and poloidal(b) magnetic field structures in the case when toroidal magnetic field rapid decreases rapidly.

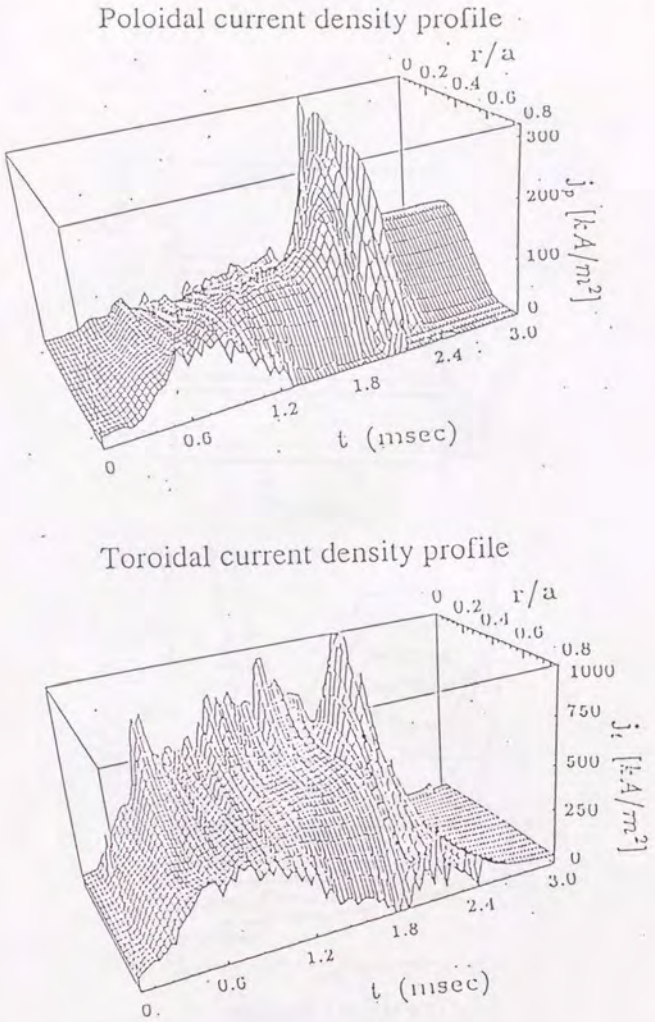

Figure 3.25: Time evolution of toroidal(a) and poloidal(b) current density profiles for the case of positive E_p pulsed experiment.

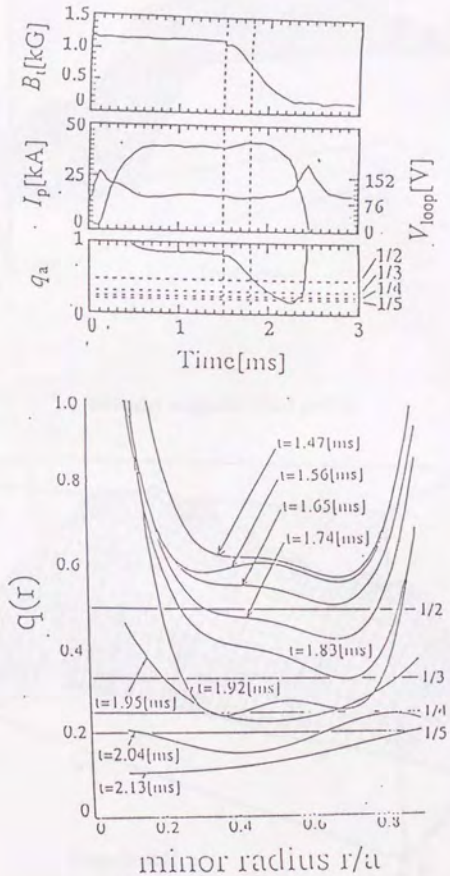

Figure 3.26: Time evolutions of plasma parameters(a) and safety factor profile(b). $q(r)$, as a function of the minor radius for the case of positive E_p pulsed experiment.

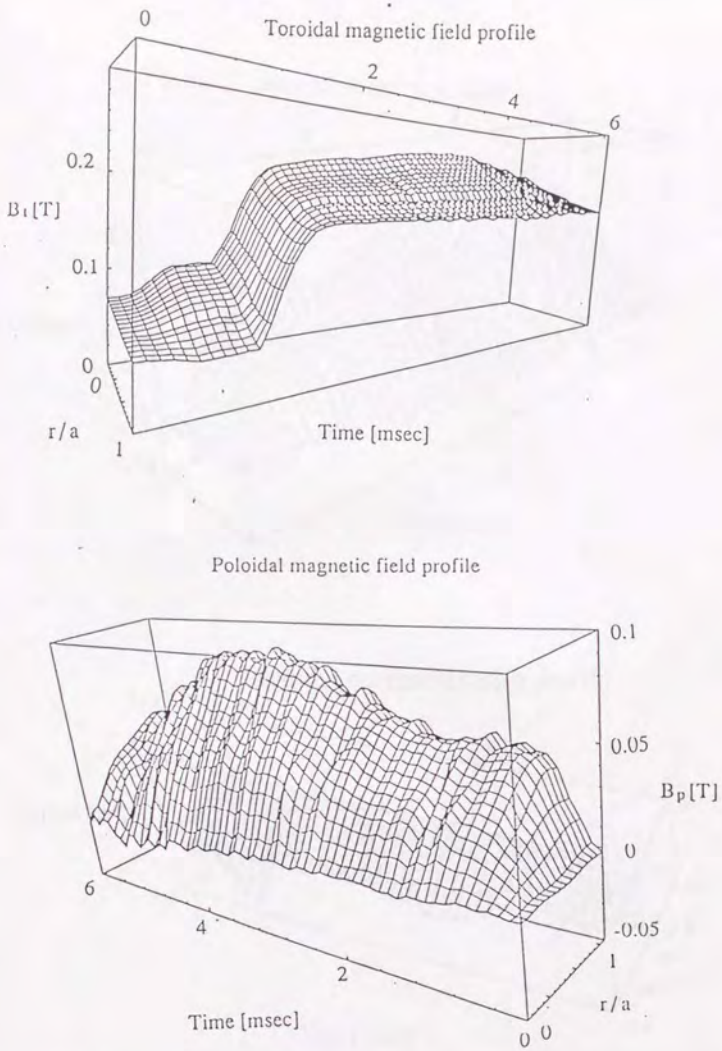

Figure 3.27: Time evolutions of toroidal(a) and poloidal(b) magnetic field structures in the case when toroidal magnetic field rapid increases rapidly.

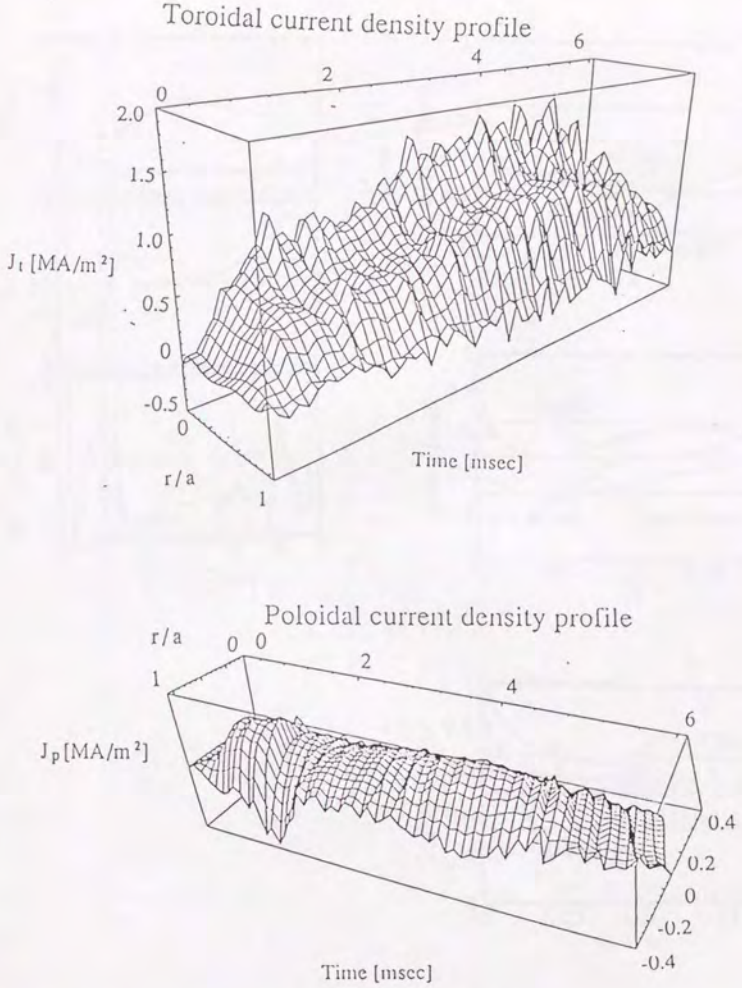

Figure 3.28: Time evolution of toroidal(a) and poloidal(b) current density profiles for the case of negative E_p pulsed experiment.

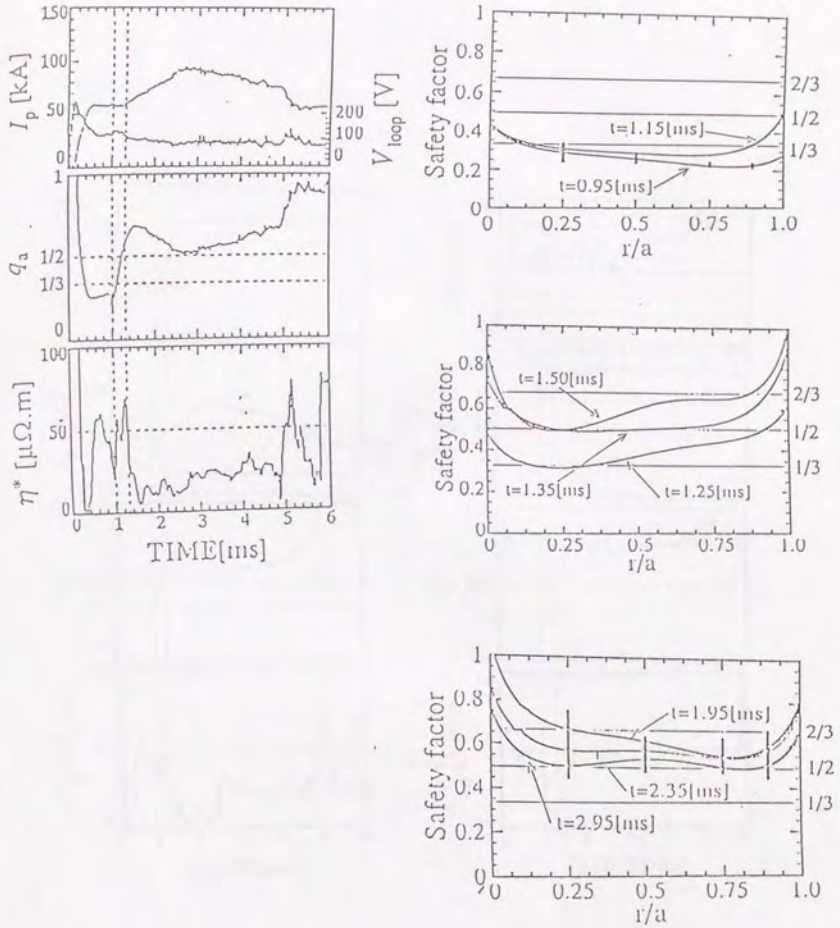

Figure 3.29: Time evolution of safety factor $q(r)$, as a function of the minor radius for the case of negative E_p pulsed experiment.

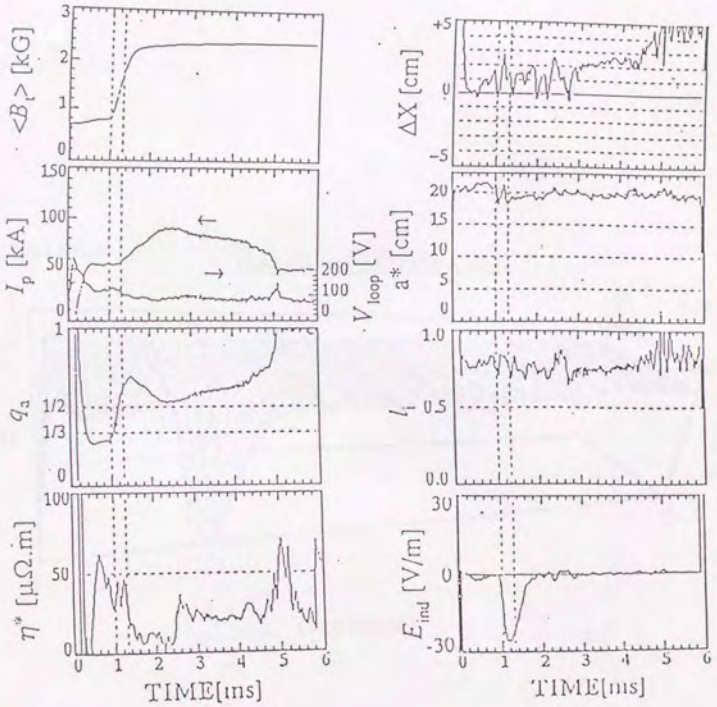

Figure 3.30: Time evolutions of plasma parameters for the case of negative E_p experiment.

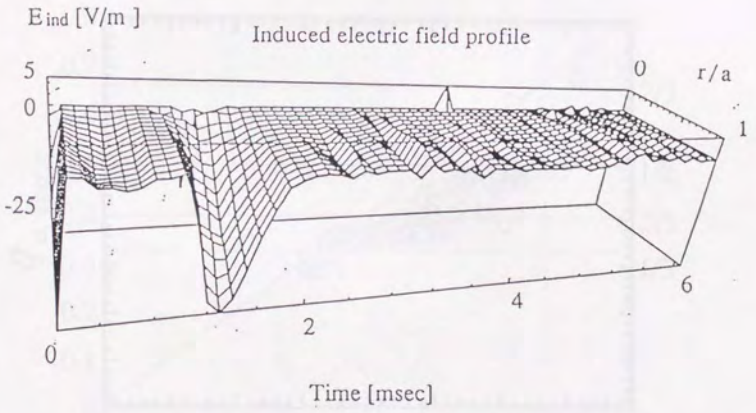

Figure 3.31: Time evolution of the induced poloidal electric field profile in the case of negative E_p pulsed experiment.

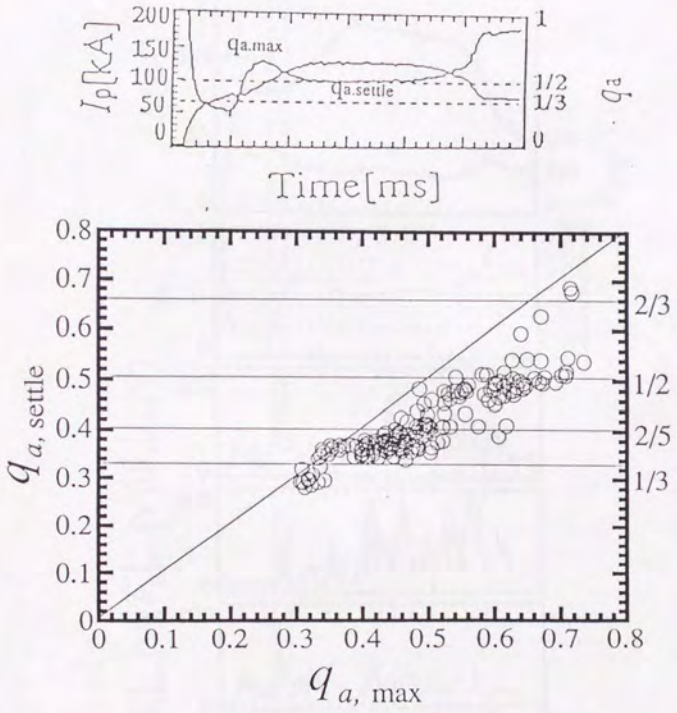

Figure 3.31: (a)Time evolutions of plasma current I_p, and safety factor at the wall q_a. (b)The safety factor at the wall just after the increase of toroidal magnetic field, $q_{a.max}$, versus the safety factor at the flat top of the plasma current $q_{a.settle}$.

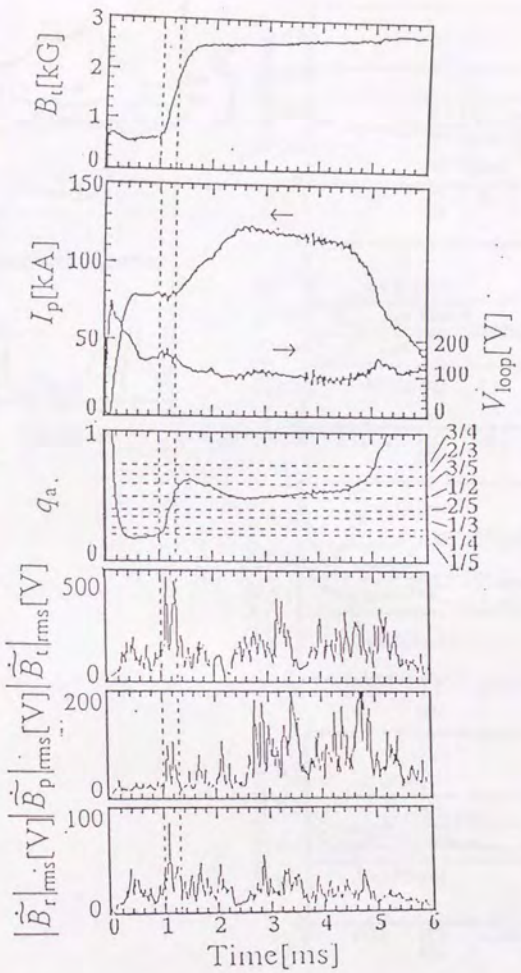

Figure 3.32: Time evolutions of magnetic toroidal magnetic field B_t, plasma current I_p, loop voltage V_{loop}, magnetic fluctuation, $|\widetilde{B}_t|_{rms}$, $|\widetilde{B}_p|_{rms}$ and $|\widetilde{B}_r|_{rms}$.

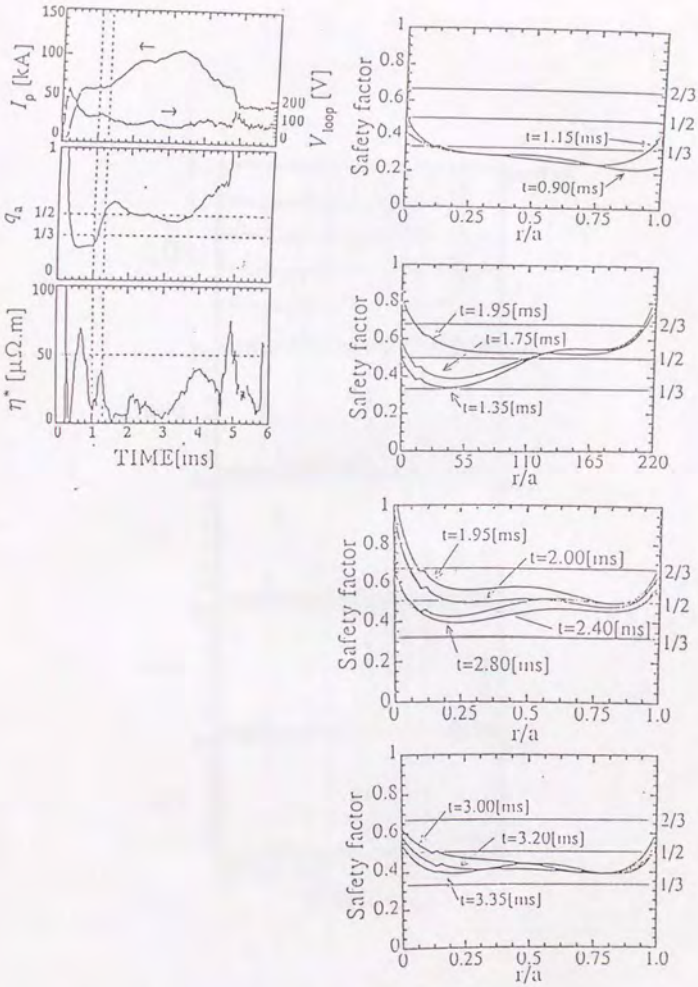

Figure 3.34: Time evolution of plasma parameters(a) and safety factor(b) in the case when plasma current increases against $q_a = 1/2$ surface.

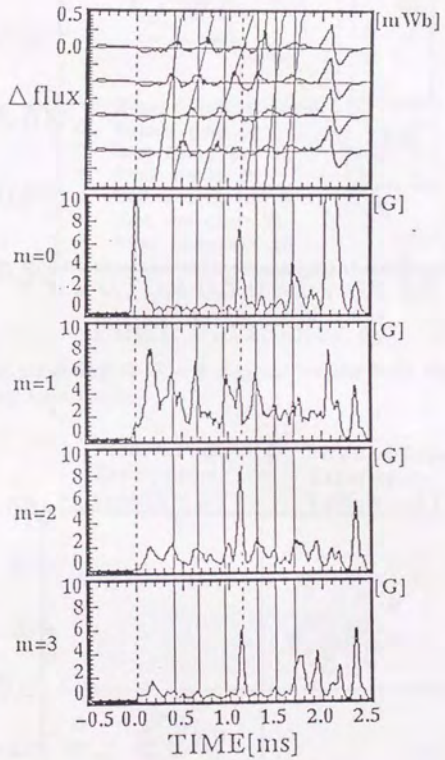

Figure 3.35: Toroidal flux perturbations at four different toroidal location and MHD mode activity for the case of E_t pulsed experiment. The diagonal line traces the motion of a flux perturbation and peak of m=1 mode.

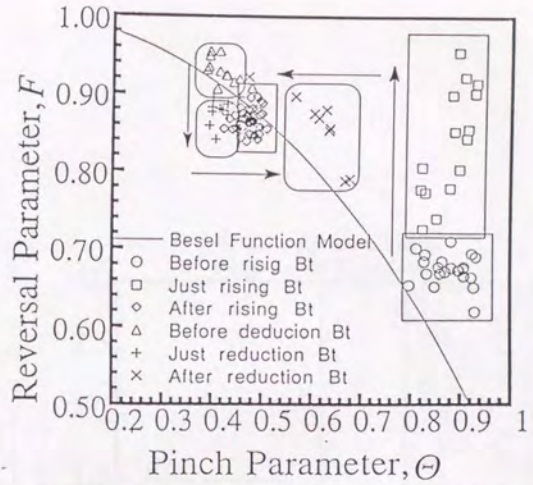

Figure 3.35: The trajectory on $F - \theta$ diagram for the both case of positive and negative E_p pulsed experiments.

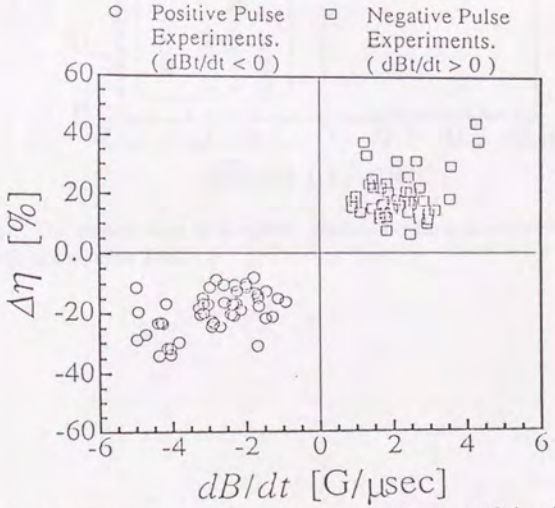

Figure 3.36: The change rate of the resistivity as a function of the change rate of toroidal magnetic field.

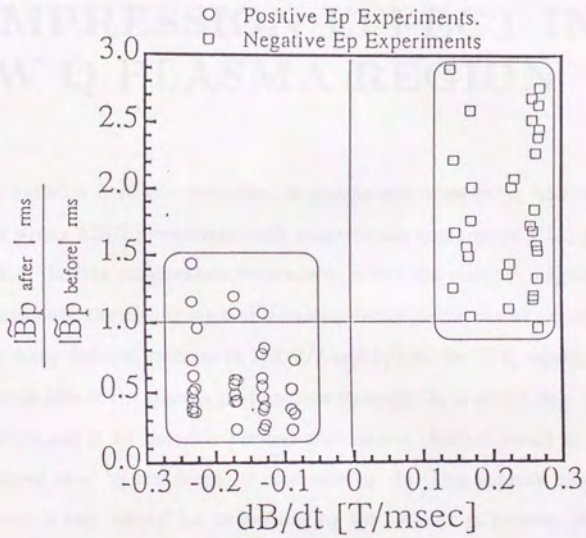

Figure 3.37: The change rate of magnetic fluctuation as a function of the change rate of toroidal magnetic field.

Chapter 4

COMPRESSION EFFECT IN LOW Q PLASMA REGION

We describe here the reduction of plasma-wall interaction and the performance of strong MHD phenomena with magnetically compressed ULQ plasmas in REPUTE-1. In this compression experiment, where the toroidal magnetic field is increased rapidly, the modification of the safety factor profile can be expected. Since there are many rational surfaces as 1/3, 1/2 and 2/3 in the ULQ region, the MHD phenomenon affects the plasma performance strongly. It is afraid that the several MHD modes might be unstable because the current channel would be free from the stabilized shell by the magnetic compression. In these aspects, the magnetic compression is very helpful for understanding the correlation between plasma-wall interaction and MHD phenomena in ULQ plasmas.

4.1 *Compression effect*

A rapid increase of toroidal magnetic field during toroidal plasma discharge brings the compression effect. Magnetic compression experiments were performed on several conventional tokamaks because adiabatic compression is a powerful tool for the generation of high pressure tokamak plasma and for the investigation of confinement characteristic of tokamak plasma. The devices for magnetic compression are presented in Table 4.1, including REPUTE-1. In these experiments, the efficiency of magnetic compression was confirmed for the conventional tokamak($q_a > 3$).

Negative E_p pulsed experiment in identical to such compression experiments and its aim is to investigate the effect of magnetic compression in low q plasma region.

The condition for adiabatic compression is required that the magnetic compression time τ_c, must be longer than the plasma relaxation time τ_{ii}, and must be shorter than the shin time of magnetic field τ_{skin} and energy confinement time τ_E,

$$\tau_{ii} << \tau_c << \tau_{skin},\ \tau_E. \tag{4.1}$$

The former condition is satisfied in REPUTE-1 compression experiment, because it is estimated to be $\tau_{ii} \sim 7\mu$sec and τ_c is $\sim 300\mu$sec. While the latter condition might be marginal, because the confinement time would be a few hundred μsec.

The compression ratio is defined as $C_a \equiv a_b/a_c$, where a_b and a_c are radii of before and after compression respectively. The change of plasma parameters are presented in Table 4.2. In compression experiment in REPUTE-1, the toroidal magnetic field rises from 1kG up to 3.5kG field. The compression ratio of this experiments is estimated about $C_a \equiv (B_c/B_b)^{1/2} = 1.87$.

4.2 *Compression Experiment in REPUTE-1*

Figure 4.1 shows that time evolutions of averaged toroidal magnetic field, $< B_t >$, and plasma minor radius, estimated from toroidal current density profile See;Fig.3.28 with the compression ratio $C_a \equiv (B_c/B_b)^{1/2} \sim 1.93$. Shrinkage of

plasma minor radius is observed. We can see that plasma minor radius tends to return immediately after the increase of toroidal magnetic field. This reason is considered to be as follows; the condition of adiabatic compression (Equation4.1) is not satisfied in these experiments and/or plasma characteristic tends to return toward standard ULQ configuration, which is current density is parallel to the magnetic flux density.(See Fig.3.28) Current density profile of ULQ and RFP is dominated by dynamo electric field and that becomes flat profile.

To study on plasma-wall interaction in the compression experiment, the eight channels fiber visible-light guide system was installed in poloidal cross-section. The interference filter of this system can change easily for various visible lines ($e.g., H_\alpha, H_\epsilon I, N_\epsilon I, ...$). The schematic drawing of this system and layout of magnetic probes is shown in Fig.3.3. The visible-light system is located at the angle of 40 degrees from the magnetic probes toroidally. To understand the plasma-wall interaction thoroughly, we use the helium gas in this experiment. Since ionized potential of helium I is $24.5eV$ and electron temperature measured by Thomson scattering is about $60eV$ at the center in the typical helium ULQ discharge, the behavior of $N_\epsilon I$ emissions show the criterion of plasma-wall interaction in the helium plasma discharge.

Figure 4.2 shows the time evolution of main plasma parameters in compressed ULQ discharge, where the toroidal magnetic field is increased from $\sim 1.0kG$ field up to $\sim 3.0kG$ field at $t = 1.0msec$. During the magnetic compression($t = 1.0 \sim 1.3msec$), the increase of the loop voltage is observed. This response can be accounted for the externally induced poloidal electric field, which direction is opposite to that of dynamo electric field [69], by a fast increase of the toroidal magnetic field. Synchronized to the magnetic compression, the remarkable reduction of the $N_\epsilon I$ emissions are observed. The intensity of $N_\epsilon I$ emissions before and after the magnetic compression is shown in Fig.4.3. This figure shows the magnetic compression is also a powerful tool for the reduction of plasma-wall interaction in low q region.

After the magnetic compression($t = 1.3 \sim 2.2msec$), the plasma current begins to increase slowly and safety factor at the wall decreases because of the improvement

the plasma characteristic due to the reduction of plasma-wall interaction and the higher toroidal field [60]. The maximum value of plasma current might be limited by large MHD activity [69].

When the rational surface appears at the plasma surface as the plasma current increases, MHD fluctuation is enhanced and strong plasma-wall interaction is observed($t = 2.0 \sim 4.5msec$). Here we observed two different types of MHD mode; One is the m=1 mode (n=2 because safety factor $q_a = m/n = 1/2$) in the region of $1/3 < q_a < 1/2$. Contour plot of the time evolution of mode spectrum for the case when m=1 mode occur, is shown in Fig.4.4. Both poloidal and toroidal mode numbers seem to cascade toward higher mode number.

Another is m=2 mode for the case when plasma current just limited on rational surface as $q_a = 1/2$. Contour plot of the time evolution of mode spectrum for the case when m=2 mode occur, is shown in Fig.4.5. Both poloidal and toroidal mode numbers does not seem to cascade toward higher mode number. The behavior of H_eI emission is different in two those types.

The behavior of H_eI emissions for the case when m=1 mode takes place

Figure 4.6(a) shows the time evolution of plasma current, safety factor at the wall and H_eI emissions through the lower(#1) and upper(#8) sides of plasma. (#1 and #8 is H_eI emission lower and upper side of plasma ,See;Fig.3.3) The low frequency oscillation of the H_eI emissions is observed and this emission is asymmetric at the lower and upper sides, where the intensity of lower side is a few times as large as that of upper sides.

The low frequency oscillation is also observed in magnetic probe signals. Oscillation patterns as observed by magnetic probes and visible light array are shown in Fig.4.6(b) with the expanded trace from $3.1msec$ to $3.9msec$. The m=1 mode is clearly observed in the signals of magnetic probe. It seems that the speed of rotation of this mode is faster when the m=1 mode moves through the outside of major radius(magnetic probe signals of %1, %2 and %3) and that direction is a

counterclockwise rotation at Fig.4.6. While, the oscillation of H_eI emissions dose not rotate with m=1 mode. However, since there is one peak of H_eI emissions in a period of m=1 mode's rotation, we can see that there is correlation between the m=1 mode's rotation and the enhancement of plasma-wall interaction.

The behavior of H_eI emissions for the case when m=2 mode takes place

The m=2 mode takes place when the decrease of the safety factor at the wall is just limited on the rational surface as 1/2. The time evolutions of plasma current, safety factor at the wall and H_eI emissions are shown in Fig.4.7(a). In this case, the enhancement of H_eI emissions is almost symmetric(#1, #8). Figure 4.8 shows that the symmetry of H_eI emission during the low frequency oscillation through the lower and upper sides of plasma as a function of the safety factor at the wall in both cases of MHD modes. This result shows the $q = 1/2$ is a strong rational surface in ULQ region. Figure 4.7(b) shows that the oscillation patterns with the expanded trace from $2.6msec$ to $3.4msec$. The m=2 mode is clearly observed by magnetic probe signals and that direction of the rotation is the same with that of m=1 mode. Since there are two peaks of H_eI emissions in a period of the m=2 mode's rotation, the behavior of H_eI emissions is caused by the m=2 mode and plasma-wall interaction is enhanced by this m=2 mode's rotation.

In those experiments, we reconfirmed that magnetic compression is also effective tool for the reduction of plasma-wall interaction in low q plasma as well as tokamak ones. After the magnetic compression, strong plasma-wall interaction is occurred accompanied by large MHD activities. Those MHD activities in compressed ULQ plasma are coherent in comparison with that in standard ULQ plasma. This reason might be considered the plasma column is modified and rotates due to the separation of the plasma surface from the wall by the magnetic compression.

For the case when m=1 mode occurs in the region of $1/3 < q_a < 1/2$, the H_eI emission is asymmetric at the lower and upper sides. The behavior of H_eI

emissions dose not rotate with the m=1 mode. However, since the visible-light guide system views the plasma radiantly(magnetic probe arrays are set up around the vacuum vessel) and there is one peak of $H_\epsilon I$ emission in a period of m=1 mode's rotation, the plasma-wall interaction might be enhanced by m=1 mode's rotation. The reason of asymmetrical plasma-wall interaction might be considered as follows; one is caused by the difference of speed of m=1 mode's rotation at the inside and outside of major radius and other is caused by the out of position of plasma column due to the magnetic compression.

While, for the case of m=2 mode occurs when the decrease of safety factor at the wall is just limited on rational surface as $q_a = 1/2$, the speed of rotation seems to be almost constant and plasma-wall interaction is symmetric. The m=2 mode might be caused by the modification of the plasma column by the magnetic compression and the plasma rotation similar to Mironov oscillation.

4.3 *Discussion and Conclusion*

To investigate the effect of magnetic compression in low q plasmas and the reduction of the plasma-wall interaction, the minor radius magnetic compression is applied in REPUTE-1 ULQ plasma. The remarkable reduction of plasma-wall interaction is observed during the magnetic compression. Shrinkage of plasma minor radius is observed. After the magnetic compression, plasma current begins to increase slowly due to the improvement of plasma characteristic. Those results show that magnetic compression is also effective tool for the reduction of plasma-wall interaction and for the improvement of plasma confinement in low q plasma as well as tokamak ones. The correlation between MHD phenomena and plasma-wall interaction is also investigated because the MHD modes are clearly observed in compressed ULQ plasmas. The different type of two MHD modes takes place and plasma-wall interaction is enhanced after the increase of the plasma current. Those modes can be distinguished on condition of the safety factor. When the safety factor is in region of $1/3 < q_a < 1/2$, the m=1 mode takes place and localized plasma-wall interaction

is enhanced. While, that is on rational surface as $q_a = 1/2$, the m=2 mode begins to dominate and symmetrical plasma-wall interaction is enhanced.

Table 4.1: Compression Device.

Device	Institute	R[m]	a[m]	B_t[T]
ATC	Princeton	$0.87 \Rightarrow 0.38$	$0.17 \Rightarrow 0.11$	2.0
Tuman-2A	Leningrad	0.40	0.08	$0.8 \Rightarrow 1.6$
Tuman-3	Leningrad	0.54	0.22	$0.5 \Rightarrow 1.0$
TOSCA	Culham	0.30	0.10	$0.3 \Rightarrow 0.6$
TFTR	Princeton	$3.15 \Rightarrow 2.10$	$0.55 \Rightarrow 0.48$	4.0
T-14/TSP		$1.10 \Rightarrow 0.40$		
ZEPHYR		$2.03 \Rightarrow 1.35$	$0.61 \Rightarrow 0.50$	$6.10 \Rightarrow 9.10$
REPUTE-1	U-Tokyo	0.82	$0.22 \Rightarrow 0.15$	$0.10 \Rightarrow 0.35$

Table 4.2: Plasma parameter with adiabatic compression.

a-compression		
Plasma Minor Radius	a	C_a^{-1}
Plasma Major Radius	R	Const.
Plasma Density	n	C_a^{2}
Temperature	T	$C_a^{4/3}$
Pressure	P	$C_a^{10/3}$
Toroidal Field	B_t	C_a^{2}
Plasma Current	I_p	Const.
Plasma Current Density	j	C_a^{2}
Safety Factor	q_a	Const.

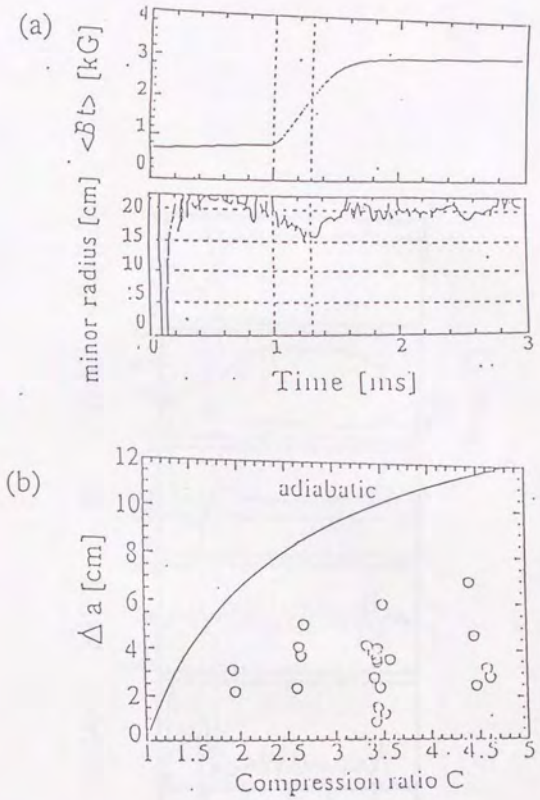

Figure 4.1: (a)Shrinkage of the plasma column in the compression experiments. Synchronized to increase of the toroidal magnetic field, we can see that plasma is shrunken from $\sim 22cm$ to $\sim 15cm$. After that plasma column seems to be returned quickly. (b) Shrinkage of the minor radius as a function of the compression ratio.

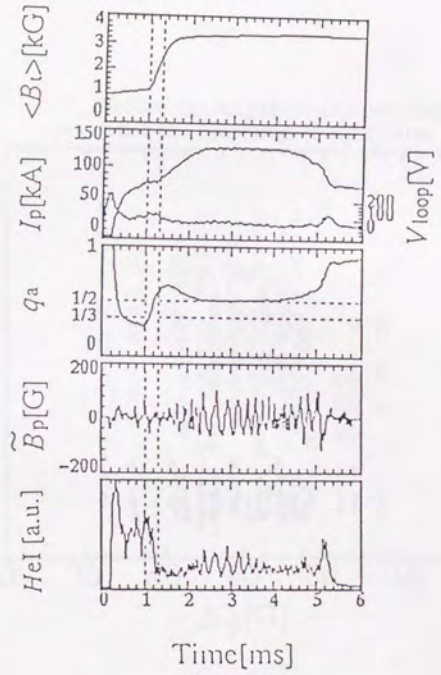

Figure 4.2: Time evolution of averaged toroidal magnetic field $< B_t >$, plasma current I_p, loop voltage V_{loop}, poloidal magnetic field fluctuation $\widetilde{B_p}$ at the plasma edge and H_eI emission on the typical magnetic compression discharge.

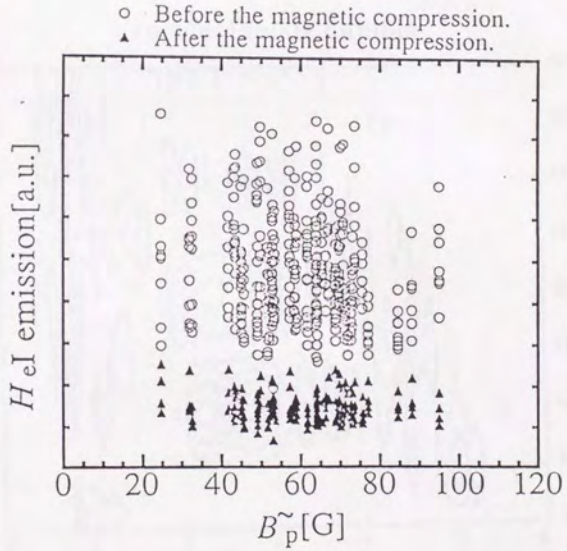

Figure 4.3: The intensity of H_eI emissions before and after the magnetic compression as a function of magnetic field.

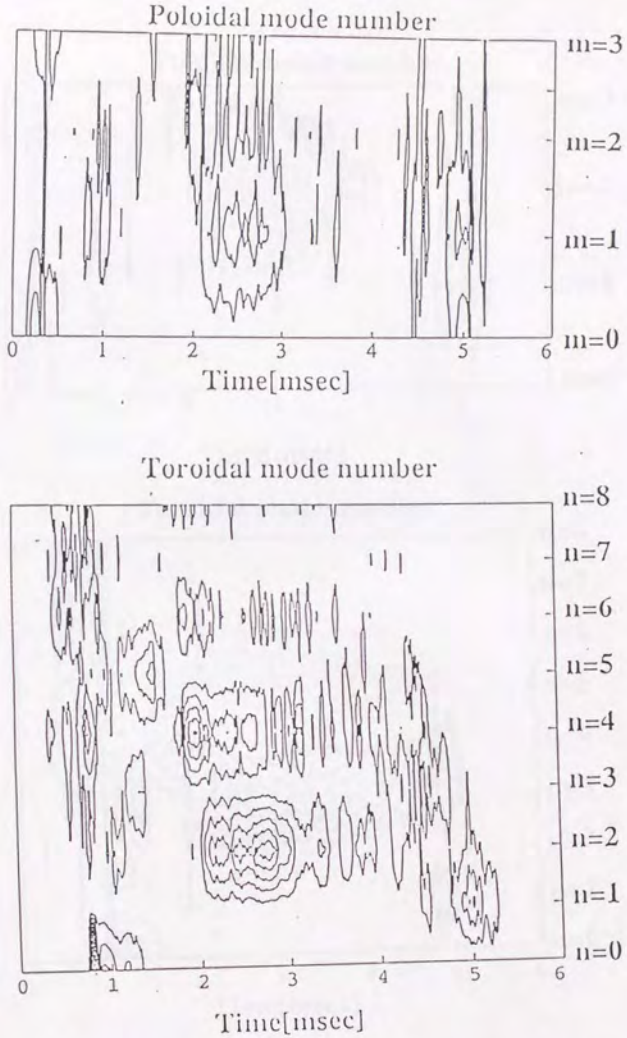

Figure 4.4: Contour plots of the time evolution of poloidal and toroidal modes. Here one mode (m,n)=(1,2) is completely dominant in the region of $1/3 < q_a < 1/2$, and both poloidal and toroidal mode numbers seem to cascade toward higher mode number.

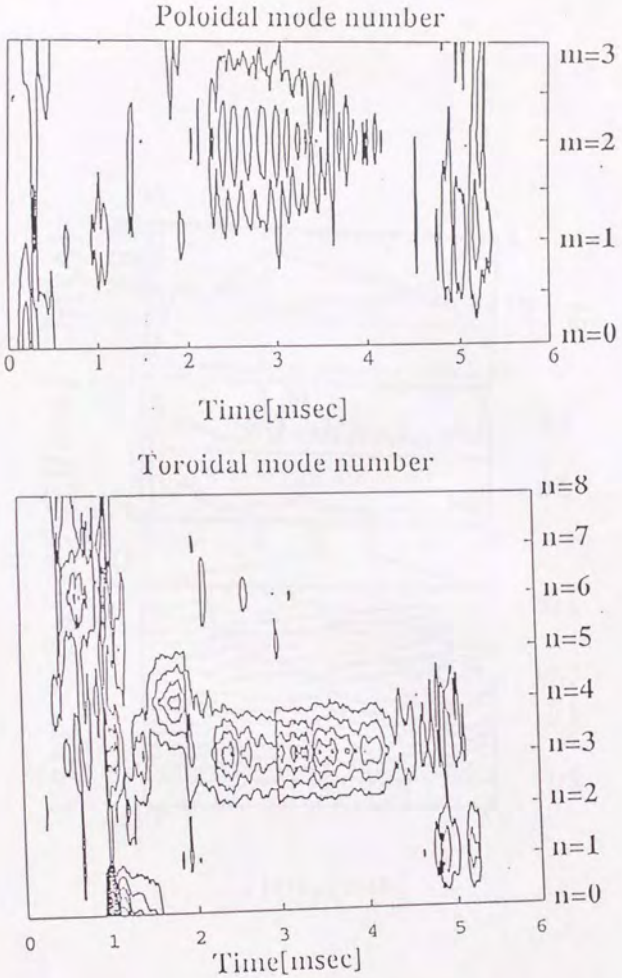

Figure 4.5: Contour plots of the time evolution of poloidal and toroidal modes. Here one mode (m,n)=(2,3) is completely dominant in the region of $1/2 < q_a$, and both poloidal and toroidal mode numbers does not seem to cascade toward higher mode number.

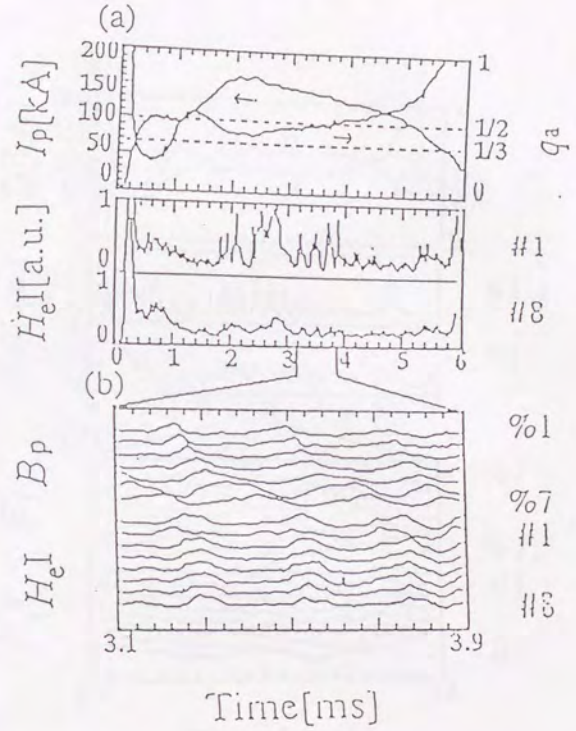

Figure 4.6: For the case when m=1 mode takes place, (a)Time evolution of plasma current, I_p, and safety factor at the wall, q_a, and H_eI emissions trough the lower(#1) and upper(#8) sides of plasma. (b)Oscillation pattern of magnetic probe signal(%1~%7) and H_eI emissions(#1~#8) during the low frequency oscillation.

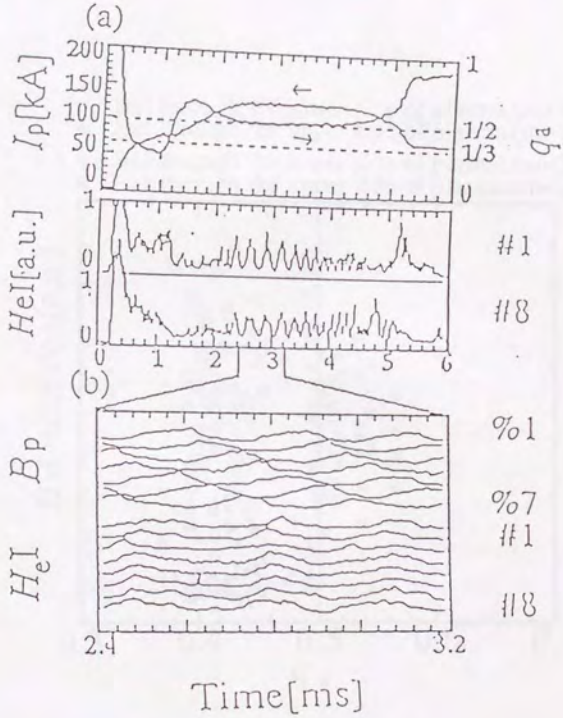

Figure 4.7: For the case when m=2 mode takes place, (a)Time evolution of plasma current I_p, and safety factor at the wall q_a, and H_eI emissions trough the lower(#1) and upper(#8) sides of plasma. (b)Oscillation pattern of magnetic probe signal(%1~%7) and H_eI emissions(#1~#8) during the low frequency oscillation.

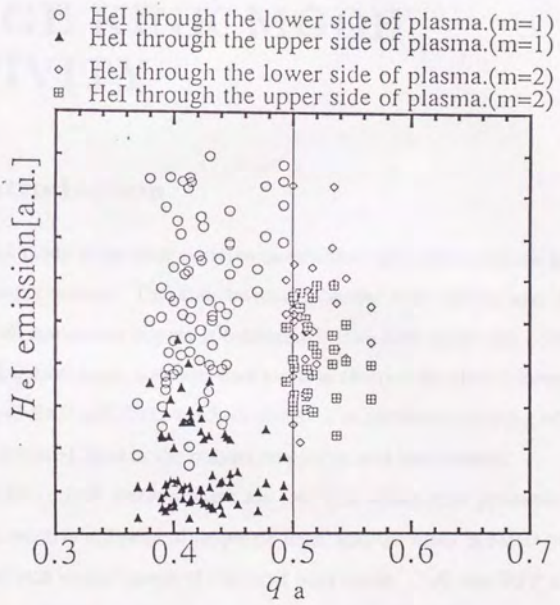

Figure 4.8: The symmetry of H_eI emissions through the lower and upper sides of plasma as a function of safety factor at the wall during the low frequency oscillations.

Chapter 5

SELF-ORGANIZATION AND LARGE KINK MODE ACTIVITY

5.1 Introduction

The kink mode is the current driven instabilities and plasma column is modified when this mode occurs. The kink instability is the most strong and dangerous instability and sometimes plasma is terminated. The kink mode also occurs in the RFP and ULQ discharges, however, such mode is effective for plasma formation and maintaining of RFP and ULQ configurations. The nonlinear coupling of the kink mode plays essential roles in the plasma relaxation and confinement.

In toroidal current system, there are two type dissipation processes. One is the classical resistive diffusion of magnetic field, and the other is MHD relaxation, accompanied with enhancement of the m=1 kink mode. ULQ and RFP configurations are self-stabilized against kink modes through such MHD relaxation and the internal magnetic profile is dominated by dynamo electric field.

5.2 Experimental Setup and Results

The stability of the m=1 kink mode is discussed by the safely factor q. In the region of $q < 1$, that is ULQ and RFP regions, the m=1 helical kink mode is enhanced and that is stabilized through self-organization process. In this region, the force free field is formed spontaneously. Such behavior is observed not only torus system, like ULQ and RFP, but also spheromak [70]. While, in the region of $q > 1$, this region is tokamak operation and safety factor q, is high more than Kruskal-Shafranov limit($q = 1$). In this region, the force free field is not formed.

In general, MHD instabilities, especially the m=1 kink mode, is stabilized by conducting shell surrounding the vacuum vessel at the ULQ and RFP. When plasma column is separated from conducting shell, for example, compression experiment or insert limiters experiment, several MHD modes will become unstable. To separate the plasma column from conducting shell, three movable limiters are installed on the toroidal arrangement. The stroke of this movable limiter is 10cm, and schematic drawing is illustrated in Fig.5.1.

To investigate the variation of internal magnetic structures, grid type of magnetic probe arrays are installed in REPUTE-1. The schematic drawing of magnetic probe arrays is shown in Fig.5.2. The magnetic probe arrays is covered by stainless steal jacket with 1.5mm thickness. The internal magnetic structure can be measured by this probe array and it is possible to investigate the variation of 2-D spatial structures of plasma parameters.

Figure 5.3 shows the time evolutions of main plasma parameters, for the case when large-kink mode occurs, in which experiment movable limiters are inserted into the plasma. Here plasma column might be partly separated from stabilized shell, this phenomena might be caused by not only movable limiters but also jacket of insert magnetic probe array. The figure shows the time evolutions of the plasma current I_p, loop voltage V_l, averaged toroidal magnetic field $< B_t >$, safety factor at the wall q_a and time differential of toroidal flux $d\psi/dt$. In this experiment, the m=1 kink

mode is enhanced actively. We can see that ULQ configuration with $I_p \sim 120kA$ and $q_a \sim 0.3$ is initially set up, and then plasma current decreases quickly with $q_a \sim 0.5$ due to the MHD relaxation. After the decrease of plasma current, the low frequency oscillations ($\sim 5kHz$) of plasma parameters are observed. We can see that many plasma parameters are influenced by large amplitude of oscillation. The oscillation of toroidal flux indicate that toroidal flux is generated by such oscillation.

Figure 5.4 shows the signals of poloidal magnetic fields measured by outside of grid type of magnetic probes array with expanded trace from 3.7msec to 4.7msec. These low frequency oscillations are identified with the m=1 kink mode. The time evolution and contour plots of poloidal mode number m, and toroidal mode number n, are shown in Fig.5.5 and Fig.5.6 respectively, where the toroidal mode number is estimated by toroidal arrangement of pick up coil located surrounding the vacuum vessel. We can see that (m,n)=(1,2) mode completely dominates on $q_a \sim 1/2$. The low mode number oscillation seems to cascade toward that of high mode number through the non linear coupling. Generally, for the non-linear coupling of MHD mode, energy of fluctuation is cascade toward the high mode number, and turbulent develops. This behavior of poloidal magnetic field is not simple oscillations, it increases slowly and decreases quickly. This results is considered to be caused by magnetic reconnection through the stabilization of the m=1 kink mode.

Figure 5.7 shows the time evolutions of low frequency oscillation, where the fluctuations of plasma current ΔI_p, loop voltage ΔV_l and toroidal flux $\Delta Flux$, are shown with the expanded trace from 3.0msec to 6.0msec. We can see that plasma parameters are oscillated, due to the enhancement of the m=1 kink mode, and toroidal magnetic field is generated in the decreasing phase of plasma current. Generally, when the toroidal current density profile is peaked due to the diffusion under ohmic heating, the safety factor at the axis decrease and the m=1 kink mode becomes unstable. This instability is caused by the decrease of the magnetic shear, due to the reduction of safety factor at the axis. When m=1 kink mode becomes unstable, the negative toroidal field component appears near the wall on the side of forward

plasma displacement, due to the solenoidal effect of the twisted plasma column.

Figure 5.8 shows the signals of radial distribution of poloidal magnetic fields with expanded trace from 3.7msec to 4.7msec. The behaviors of magnetic field oscillation are remarkable different between inside(r=106mm) and outside(r=210mm) during a typical relaxation phase. In this discharge, since current channel is partly separated from the wall, we can see the enhancement and self stabilization of the m=1 kink mode clearly. During t=4.2 $\sim$ 4.6ms, the increase of the poloidal magnetic field at the outside of the plasma is observed, while the poloidal magnetic field at the inside of plasma is decreased slowly. In this phase, plasma current density becomes flat profile. After then, poloidal magnetic field is changed instantaneously. The decrease of the poloidal magnetic field at the outside, and increase of the poloidal magnetic field at the inside are observed. In this phase, plasma current density becomes peak profile. This peak profile of plasma current density becomes flat profile, due to the self stabilization of the m=1 kink mode. Thus, peak and flat profiles of plasma current density profile is repeated. Figure 5.9 shows the time evolution of toroidal current density contours derived from multi-channel magnetic probe data during the enhancement of the large kink instability. We can see the process of the enhancement and self stabilization of the m=1 kink instability. The think line traces the plasma current density in the region more than $0.2MA/m^2$. The m=1 kink mode is self stabilized during t=3.3 $\sim$ 3.4 msec (See:Fig.5.5). After then is is enhanced during t=3.6 $\sim$ 3.9 msec and it is self stabilized again and such process is repeated.

5.3 Discussion and Conclusion

To investigate the correlation of self-organization and kink instabilities, the multi-channel magnetic probe is installed on REPUTE-1. In general, ULQ plasma is stabilized by conducting shell surrounding the vacuum vessel. In this experiment, to enhance the kink mode actively, plasma is separated from the conduction shell with the use of inserted movable limiters. In this experiment, the large amplitude

oscillation of the plasma parameters are observed.

This low frequency oscillation is identified to the (m,n)=(1,2) kink mode on the safety factor $q_a \sim 1/2$. The behavior of magnetic field oscillation is remarkably different between inside(r=106mm) and outside(r=210mm) during a typical relaxation phase, and this behavior is not simple oscillation. When the magnetic field at the outside of plasma decreases, the increase of the magnetic field is observed at the inside plasma region simultaneously. Those results can be explained as follows

1. Force free field is formed at the initial phase. In those phase, current density profile is formed almost flat, due to the dynamo electric field.

2. For the diffusion under the ohmic heating, current density profile becomes peak, that is, the safety factor at the axis decrease. In this experiment, the m=1 kink mode becomes unstable, since plasma column is separated from the stabilized shell.

3. The m=1 kink mode is self stabilized spontaneously through the dynamo effect. After then flat profile of current density profile is formed.

4. Current density profile becomes peak due to the diffusion under the ohmic heating and the m=1 kink mode is enhanced again.

Thus, those flat and peak profiles of current density are repeated through the correlation of dynamo effect and the self stabilization of the m=1 kink instabilities.

Since such behavior of magnetic field, it is anticipated that the magnetic reconnection process occurs in this experiment (m=1 kink driven reconnection). The current profile becomes more flat slowly and the plasma relaxes into a more stable state. Since the current profile is peaked due to the diffusion under the ohmic heating. Thus peak and flat profiles of plasma current are repeated through the enhancement and self stabilization of the m=1 kink instabilities. Those behavior is a one of the self-organization process.

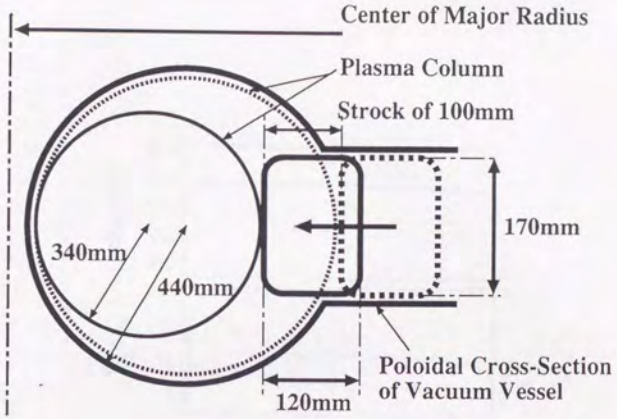

Figure 5.1: Layout of movable limiter.

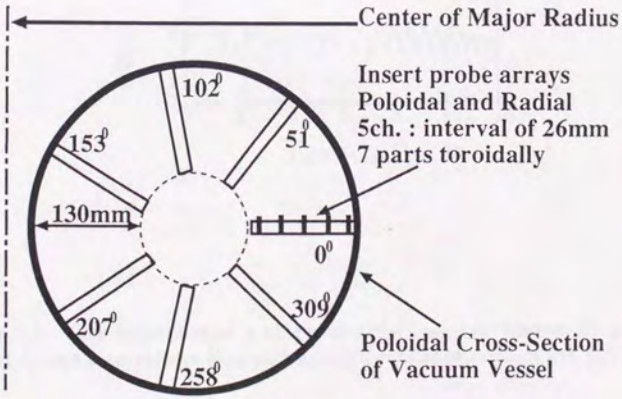

Figure 5.2: Schematic drawing of grid type of internal probe array.

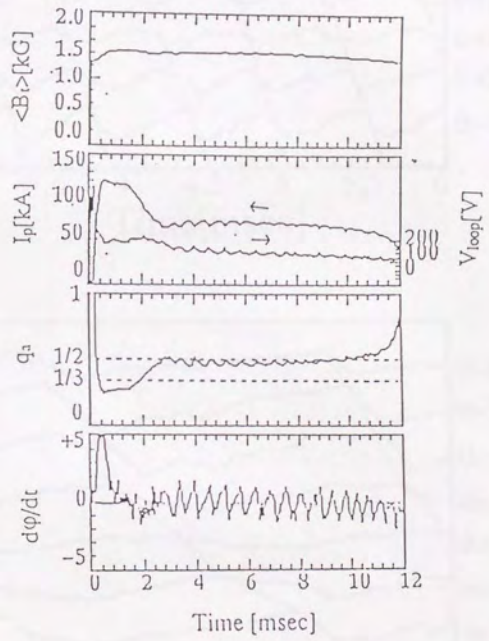

Figure 5.3: Time evolutions of averaged toroidal magnetic field $< B_t >$, plasma current I_p, one turn voltage V_{loop} and time differential of toroidal flux $d\varphi/dt$.

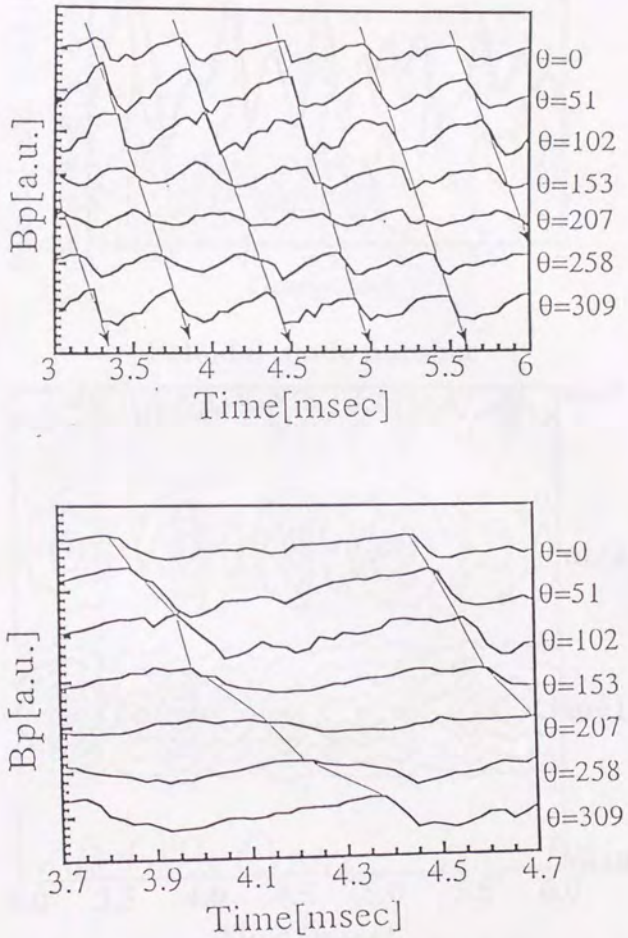

Figure 5.4: The signal of poloidal magnetic fields measured by outside of grid type magnetic probes arrays with expanded trace from 3.7msec to 4.7msec.

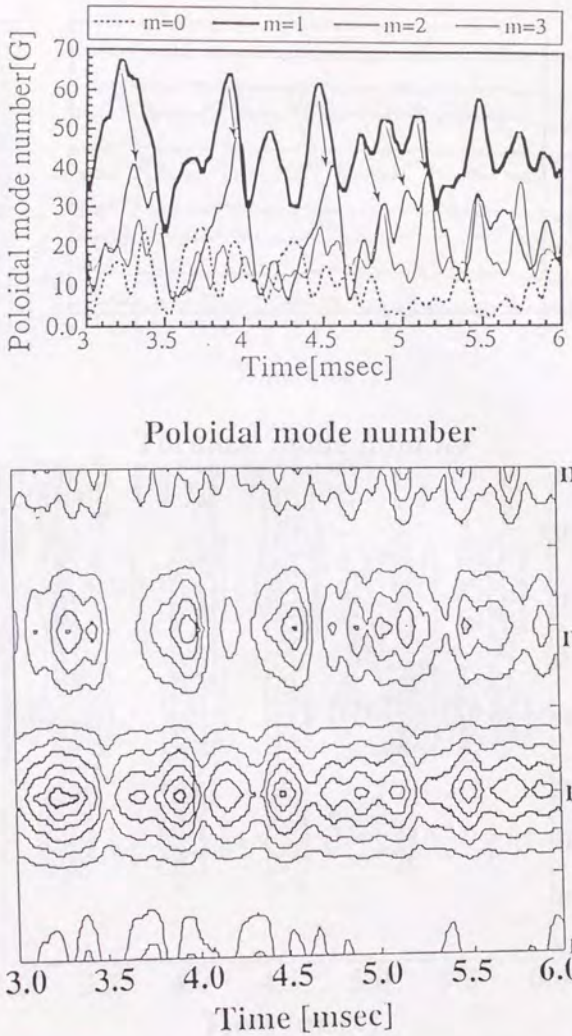

Figure 5.5: (a)Time evolution of poloidal mode numbers m and (b)Contour plot of the time evolution of poloidal mode number during low frequency oscillation. Here one mode m=1 is completely dominant in the region of $q_a \sim 1/2$.

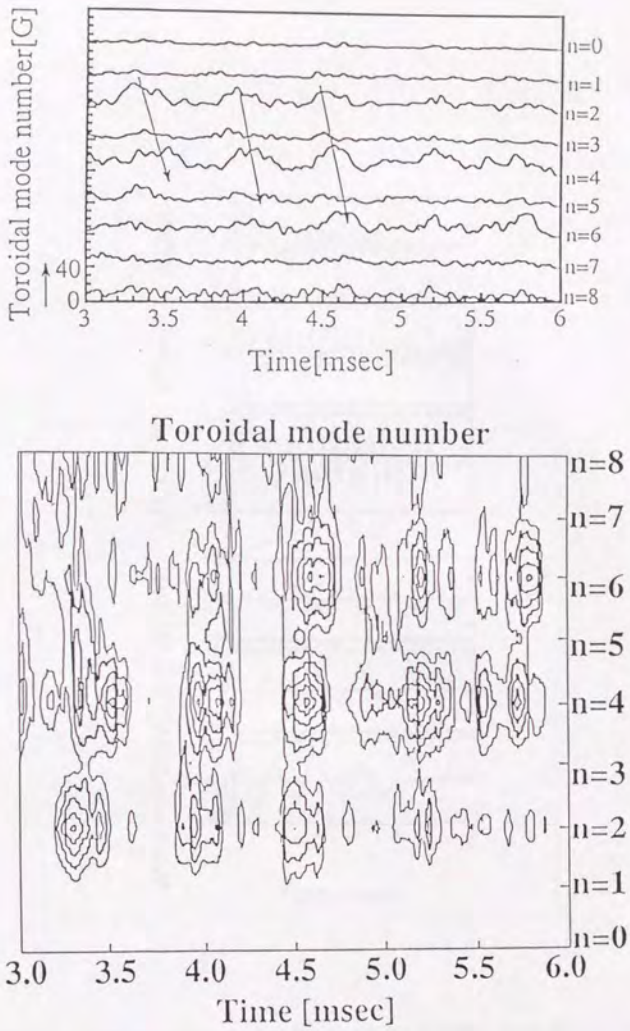

Figure 5.6: (a)Time evolution of toroidal mode numbers n and (b)Contour plot of the time evolution of toroidal mode number during low frequency oscillation. Here one mode n=2 is completely dominant in the region of $q_a \sim 1/2$.

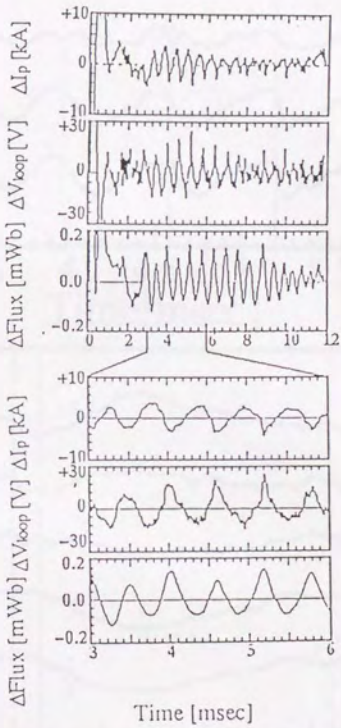

Figure 5.7: Time evolutions of low frequency oscillation, where the fluctuations of plasma current ΔI_p, loop voltage ΔV_l and toroidal flux $\Delta Flux$, are shown, with the expanded trace from 3.0msec to 6.0msec.

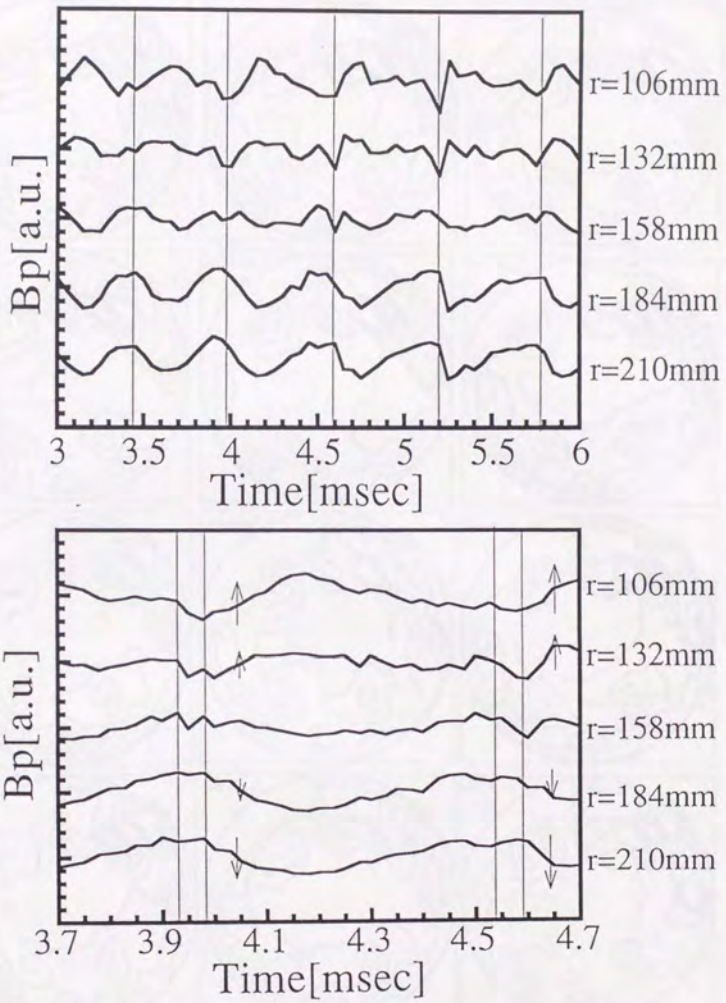

Figure 5.8: The signal of poloidal magnetic fields measured by inside of grid type magnetic probes arrays, with expanded trace from 3.7msec to 4.7msec.

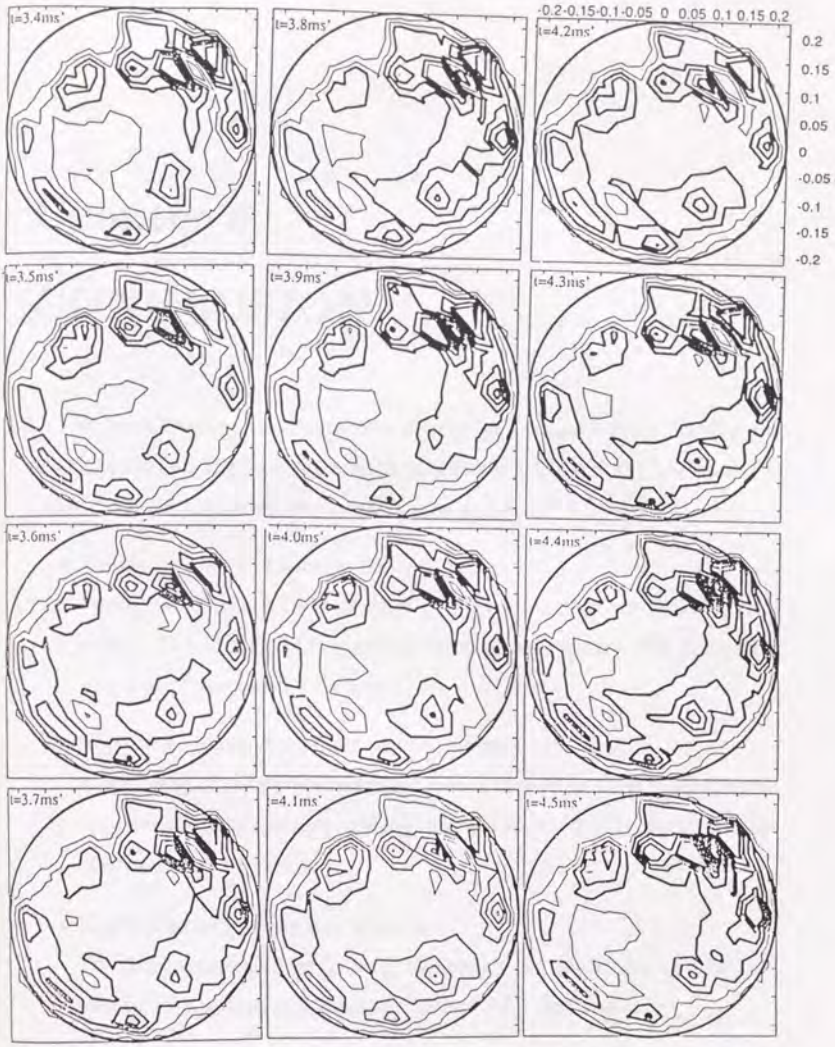

Figure 5.9: Time evolution of toroidal current density contours from multi-channel magnetic probe date during the enhancement and self stabilization of the m=1 kink mode.

Chapter 6

CONCLUSION

To investigate the self-organization process and dynamo activity, toroidal and poloidal pulsed electric fields are applied on standard ULQ and RFP plasmas. The pulsed electric fields are induced by three ways as follows;

- Positive E_p pulsed experiment on ULQ plasma.
  During the standard ULQ discharge, the toroidal magnetic field decreases rapidly. The direction of externally-induced poloidal electric field is the same with that of dynamo electric field.

- Negative E_p pulsed experiment on ULQ plasma.
  A fast rising of the toroidal magnetic field is applied on ULQ plasma, where the direction of the externally-induced poloidal electric field is opposite to that of dynamo electric field.

- E_t pulsed experiment on RFP plasma.
  The positive toroidal electric field, induced by the application of additional toroidal loop voltage, is applied on standard RFP discharges.

In these experiments, synchronized to the applications of the pulsed electric fields, the remarkable responses of the several plasma parameters are observed. Table 6.1 shows the experimental results during the transient phase and after the transient phase.

Table 6.1: Plasma Responses on Toroidal and Poloidal Pulsed Electric Fields.

Transient phase	Positive E_p	Negative E_p	E_t
Plasma Current I_p	$\uparrow$	$\rightarrow$	$\uparrow$
Loop Voltage V_l	$\downarrow$	$\nearrow$	$\uparrow$
Averaged toroidal flux $< B_t >$	$\downarrow$	$\nearrow$	$\uparrow$
Fluctuation $\tilde{B}$	$\searrow$	$\uparrow$	$\rightarrow$
Plasma resistance η^*	$\downarrow$	$\nearrow$	$\nearrow$
Pinch Parameter θ	$\rightarrow$	$\rightarrow$	$\rightarrow$
Reversal Parameter F	$\searrow$	$\uparrow$	$\rightarrow$
After the transient phase			
Plasma Current I_p	$\uparrow$	$\uparrow$	$\searrow$
Loop Voltage V_l	$\downarrow$	$\downarrow$	$\searrow$
Averaged toroidal flux $< B_t >$	$\rightarrow$	$\rightarrow$	$\searrow$
Fluctuation $\tilde{B}$	$\searrow$	$\downarrow$	$\rightarrow$
Plasma resistance η^*	$\downarrow$	$\downarrow$	$\searrow$
Pinch Parameter θ	$\uparrow$	$\downarrow$	$\rightarrow$
Reversal Parameter F	$\downarrow$	$\uparrow$	$\rightarrow$

† Transient Phase.

- For the case of positive and negative E_p pulsed experiments, just after the applications of the induced electric fields, reversal parameter F is slipped out of experimental scaling of $F-\theta$ curve with constant of pinch parameter θ, and then such slipped parameters are returned near the experimental scaling immediately. Those results indicate that configuration of force free field is strong. When spatial structure of magnetic field was changed by the external forces, plasma characteristics is returned to original state (force free field) through the self organization immediately.
- For the case of positive E_p pulsed experiment, plasma resistance is reduced, accompanied with the reduction of magnetic fluctuations. In this experiment, F and θ values change toward the theoretical model of BFM.

When the change of F value is enough to large, in this state, it is slipped out of BFM, the magnetic fluctuation tends to be enhanced.

While for the case of negative E_p pulsed experiment, increase of plasma resistance, accompanied with the enhancement of magnetic fluctuations, is observed, since F value slips out of the BFM.

The dynamo electric field, which is strong coupled with plasma fluctuations, is considered to be partly replaced or enhanced by the induced poloidal electric fields.

- For the case of E_t pulsed experiment, synchronized to the increase of toroidal plasma current, the remarkable increase of the averaged toroidal magnetic field is observed. Reversal parameter F and pinch parameter θ are almost kept constant with regard to any change of plasma parameters.

  This result indicates the poloidal current density is converted by induced toroidal electric field through the dynamo effect.

† After the transient phase

- Reversal parameter F, and pinch parameter θ moves on the BFM against any plasma verifications.
- Poloidal magnetic field is generated by induced toroidal magnetic field in E_p pulsed experiments, and toroidal magnetic field is converted by induced poloidal magnetic field in E_t pulsed experiment.

  These results indicate the experimental verification of the closed circle of dynamo effect.

  $B_t \Rightarrow (dynamo\ effect) \Rightarrow j_t$

  $j_t \rightarrow (Ampère's\ law) \rightarrow B_p$

  $B_p \Rightarrow (dynamo\ effect) \Rightarrow j_p$

  $j_p \rightarrow (Ampère's\ law) \rightarrow B_t$

  $B_t \Rightarrow .$

To investigate the effect of magnetic compression in low q plasma regions and the reduction of the plasma-wall interaction, the negative E_p pulsed experiment has been performed. This experiment is equivalents to minor radius compression experiment. In this experiment, the remarkable reduction of plasma-wall interaction is observed during the magnetic compression. The shrinkage of plasma column is also observed. After the magnetic compression, plasma current begins to increase slowly due to the improvement of plasma characteristic. Those results show that magnetic compression is also effective tool for the reduction of plasma-wall interaction and for the improvement of plasma confinement in low q plasma as well as tokamak ones.

The correlation between the MHD instabilities and plasma-wall interaction are also investigated. Since the plasma column is detached from the stabilized shell after the magnetic compression, the MHD modes are enhanced in compressed ULQ plasmas. The different type of two MHD modes takes place and plasma-wall interaction is enhanced after the increase of the plasma current. Those modes are distinguished on the condition of the safety factor. When the safety factor is in the region of $1/3 < q_a < 1/2$, (m,n)=(1,2) mode takes place and localized plasma-wall interaction is enhanced. While, that is limited on rational surface as $q_a = 1/2$, (m,n)=(2,3) mode begins to dominate and symmetrical plasma-wall interaction is enhanced.

To investigate the correlation of self-organization and kink instabilities, the multi-channel magnetic probe is installed on REPUTE-1. In general, ULQ plasma is stabilized by conducting shell surrounding the vacuum vessel. To enhance the kink mode actively, plasma is separated from the conduction shell with the use of inserted movable limiters. In this experiment, the large scale oscillations of the plasma parameters are observed. This low frequency oscillation of plasma parameters are identified to the (m,n)=(1,2) kink mode on the safety factor $q_a \sim 1/2$.

The plasma parameters are oscillated due to the enhancement of the m=1 kink mode. When the m=1 kink mode becomes unstable, the negative toroidal field component appears near the wall on the side of forward plasma displacement due to the solenoidal effect of the twisted plasma column. The behavior of 2-D toroidal current density profile is investigates using the multi-channel magnetic probe. In those discharges flat and peak profiles of current density are repeated through the enhancement and self stabilization process of the kink instability. Those behavior is a one of the self-organization process.

Bibliography

[1] J.A.Wesson. *Nucl. Fusion*, 18:87–132, 1978.

[2] M. Keilhacker et al. In *Plasma Physics and Controlled Nuclear Fusion Research 1992 (Proc. 14th Int. Conf. Wurzburg. 1992) Vol.1.*, pages 15–40, 1992.

[3] T.C.Simonen et al. In *Plasma Physics and Controlled Nuclear Fusion Research 1992 (Proc. 14th Int. Conf. Wurzburg. 1992) Vol.1.*, pages 41–55, 1992.

[4] M.Shimada et al. In *Plasma Physics and Controlled Nuclear Fusion Research 1992 (Proc. 14th Int. Conf. Wurzburg. 1992) Vol.1.*, pages 57–77, 1992.

[5] L.Laurent et al. In *Plasma Physics and Controlled Nuclear Fusion Research 1992 (Proc. 14th Int. Conf. Wurzburg. 1992) Vol.1.*, pages 79–97, 1992.

[6] A.Gibson et al. In *Plasma Physics and Controlled Nuclear Fusion Research 1992 (Proc. 14th Int. Conf. Wurzburg. 1992) Vol.1.*, pages 99–109, 1992.

[7] M.C.Zarnstorff et al. In *Plasma Physics and Controlled Nuclear Fusion Research 1992 (Proc. 14th Int. Conf. Wurzburg. 1992) Vol.1.*, pages 111–125, 1992.

[8] W.Koppendorfer et al. In *Plasma Physics and Controlled Nuclear Fusion Research 1992 (Proc. 14th Int. Conf. Wurzburg. 1992) Vol.1.*, pages 127–140, 1992.

[9] S.C.Prager et al. In *Plasma Physics and Controlled Nuclear Fusion Research 1992 (Proc. 14th Int. Conf. Wurzburg. 1992) Vol.2.*, pages 531–537, 1992.

[10] S.A.Hokin et al. In *Plasma Physics and Controlled Nuclear Fusion Research 1992 (Proc. 14th Int. Conf. Wurzburg. 1992) Vol.2.*, pages 539–545, 1992.

[11] H.Toyama et al. In *Plasma Physics and Controlled Nuclear Fusion Research 1992 (Proc. 14th Int. Conf. Wurzburg. 1992) Vol.2.*, pages 547–552, 1992.

[12] D.D.Scnack et al. In *Plasma Physics and Controlled Nuclear Fusion Research 1992 (Proc. 14th Int. Conf. Wurzburg. 1992) Vol.2.*, pages 553–559, 1992.

[13] J.P.Wainwright et al. In *Plasma Physics and Controlled Nuclear Fusion Research 1992 (Proc. 14th Int. Conf. Wurzburg. 1992) Vol.2.*, pages 561–566, 1992.

[14] RFX TEAM. In *Plasma Physics and Controlled Nuclear Fusion Research 1992 (Proc. 14th Int. Conf. Wurzburg. 1992) Vol.2.*, pages 583–595, 1992.

[15] Y.Yagi et al. In *Plasma Physics and Controlled Nuclear Fusion Research 1992 (Proc. 14th Int. Conf. Wurzburg. 1992) Vol.2.*, pages 611–617, 1992.

[16] N. Asakura, N. Fujisawa, et al. In *Plasma Physics and Controlled Nuclear Fusion Research 1986 (Proc. 11th Int. Conf. Baltimore. 1986) Vol.2.*, page 433, 1987.

[17] R. G. Watt and R. A. Nebel. *Rhys. Fluid.*, 26:1168, 1983.

[18] K. A. Werley, R. A. Nebel, and G. A. Wurden. *Rhys. Fluid.*, 28:1450, 1985.

[19] R. B. Howell, J. C. Ingraham, et al. *Rhys. Fluid.*, 30:1828, 1987.

[20] Z. Yoshida et al. *J. Phys. Soc. Jpn.*, 55:450, 1986.

[21] H. Yamada et al. *Nucl. Fusion*, 27:1169, 1987.

[22] P. L. Taylor et al. *Nucl. Fusion*, 29:92, 1989.

[23] Y. Kamada et al. *Nucl. Fusion*, 29:713, 1989.

[24] H. Y. W. Tsui et al. *Nucl. Fusion*, 30:59, 1990.

[25] J. B. Taylor. *Rhys. Rev.*, 33:1136, 1974.

[26] M. Steenbeck, F. Krause, et al. *Rhys. Rev.*, 75:1169, 1949.

[27] Z.Yoshida. *Journal of Plasma and Fusion Resarch*, 64:58, 1990.

[28] S.von Goeler et al. *Rhys. Rev.Lett.*, 33:1201, 1974.

[29] D.J.Campbell et al. *Nucl. Fusion*, 26:1085, 1986.

[30] W.Pfeiffer et al. *Nucl. Fusion*, 25:655, 1985.

[31] K.McGuire et al. In *Plasma Physics and Controlled Nuclear Fusion Research 1986 (Proc. 11th Int. Conf. Kyoko. 1986) Vol.1.*, page 421, 1986.

[32] R.Lust et al. *Kraftfreie Magnetfelder.Z.Astrophys.*, 34:263–282, 1954.

[33] N. Inoue et al. In *Plasma Physics and Controlled Nuclear Fusion Research 1988 (Proc. 15th Int. Conf. Nice. 1988).*, page 671, 1988.

[34] T. Fujita et al. *Nucl. Fusion*, page 3, 1991.

[35] K.Bol et al. In *Plasma Physics and Controlled Nuclear Fusion Research 1974 (Proc. 5th Int. Conf. Tokyo. 1974).*, page 77, 1974.

[36] G.Tait et al. In *Plasma Physics and Controlled Nuclear Fusion Research 1988 (Proc. 12th Int. Conf. Nice. 1988).*, page 141, 1988.

[37] T. Yu. Akatova et al. In *Heating in Toroidal Plasma (Proc. of Int. Symposium Grenoble, Joint Varenna Grenoble 1978).*, page 985, 1978.

[38] T. Yu. Akatova et al. In *Plasma Physics and Controlled Nuclear Fusion Research 1990 (Proc. 13th Int. Conf. Nice. 1990).*, page 509, 1990.

[39] E. N. Paker. *Astrophys.J.*, page 383, 1966.

[40] M. Steenbeck, F. Krause, et al. *Z.Naturf.*, page 369, 1966.

[41] L .Woltjer. A theorem on forece free magnetic field. *Proc. Natl. Acad. Scic, USA*, 44:489, 1958.

[42] D.R.Wells et al. *Journal of Plasma Physics*, 3:21, 1969.

[43] S. Chandrasekhar et al. On force free magnetic field. *Proc. Natl. Acad. Scic, USA*, 44:285, 1958.

[44] J .B .Taylor. In *Plasma Physics and Controlled Nuclear Fusion Research 1974 (Proc. 15th Int. Conf. Tokyo. 1974). Vol.1*, page 161, 1974.

[45] J .B .Taylor. In *Pulsed High Bete Plasma, Proc. of the Third Topical Conf. Abington*, page 59, 1976.

[46] Z.Yoshida et al. In *Plasma Physics and Controlled Nuclear Fusion Research 1984 (Proc. 10th Int. Conf. London. 1984). Vol.2*, page 467, 1985.

[47] K.Miyamoto and J.A.Wesson. In *Plasma Science(Proc. IEEE Int. Conf. Saskatoon 1986. IEEE, New York*, page 2, 1986.

[48] E.J.Caramena et al. *Phys. Fluid*, page 1305, 1983.

[49] K.Kusano et al. *Nucl. Fusion*, 26:1051, 1986.

[50] A.Bhattacharjee et al. *Rhys. Rev.*, 45:347, 1980.

[51] T.Sato et al. *Rhys. Rev.*, 54:54, 1985.

[52] K.Miyamoto. *Nucl. Fusion*, 25:1687, 1985.

[53] A.Sykes and J.A.Wesson. In *Proc. 8th Europ. Conf. on controlled Fusion and Plasma Physics. 1977. Vol.1*, page 80, 1977.

[54] D. A. Baker et al. In *Plasma Physics and Controlled Nuclear Fusion Research 1982 (Proc. 9th Int. Conf. Baltimore. 1982). Vol.1*, pages 587–595, 1982.

[55] H. A. B. Bodin et al. In *Plasma Physics and Controlled Nuclear Fusion Research 1982 (Proc. 9th Int. Conf. Baltimore. 1982). Vol.1*, pages 641–657, 1982.

[56] T. Tamano et al. In *Plasma Physics and Controlled Nuclear Fusion Research 1982 (Proc. 9th Int. Conf. Baltimore. 1982). Vol.1*, pages 609–618, 1982.

[57] V. Antoni et al. In *Plasma Physics and Controlled Nuclear Fusion Research 1982 (Proc. 9th Int. Conf. Baltimore. 1982). Vol.1*, pages 619–640, 1982.

[58] J. B. Taylor. *Reviews of Modern Physics.*, 58(3):741, 1986.

[59] T. Yu. Akatova et al. In *Plasma Physics and Controlled Nuclear Fusion Research 1990 (Proc. 13th Int. Conf. Nice. 1990).*, page 509, 1990.

[60] Z. Yoshida et al. *Nucl. Fusion*, page 1532, 1991.

[61] K. Saito et al. In *Proc. 20th Europ. Conf. on controlled Fusion and Plasma Physics. 1993. Vol.2*, pages 479–482, 1993.

[62] H.Arimoto et al. *J.Phys.Soc.Jpn.*, page 1232, 1985.

[63] R.B.Howell et al. *Phys. Fluids*, page 1828, 1987.

[64] K.Hattori et al. *J.Phys.Soc.Jpn.*, page 24, 1989.

[65] Z. Yoshida et al. *Phis. Fluids*, page 2465, 1987.

[66] H. A. B. Bodin, A. A. Newton, et al. *Nucl. Fusion*, page 1255, 1980.

[67] V. Antoni, S. Ortolani, et al. *Plasam Phys.*, page 799, 1983.

[68] R. J. La. Haye, T. N. Carlstrom, et al. *Phys. Fluids*, page 2576, 1984.

[69] M. Watanabe et al. In *Proc. 20th Europ. Conf. on controlled Fusion and Plasma Physics. 1993. Vol.2*, pages 507–510, 1993.

[70] Y. Ono et al. *Rhys. Rev.Lett.*, 61:2847, 1988.

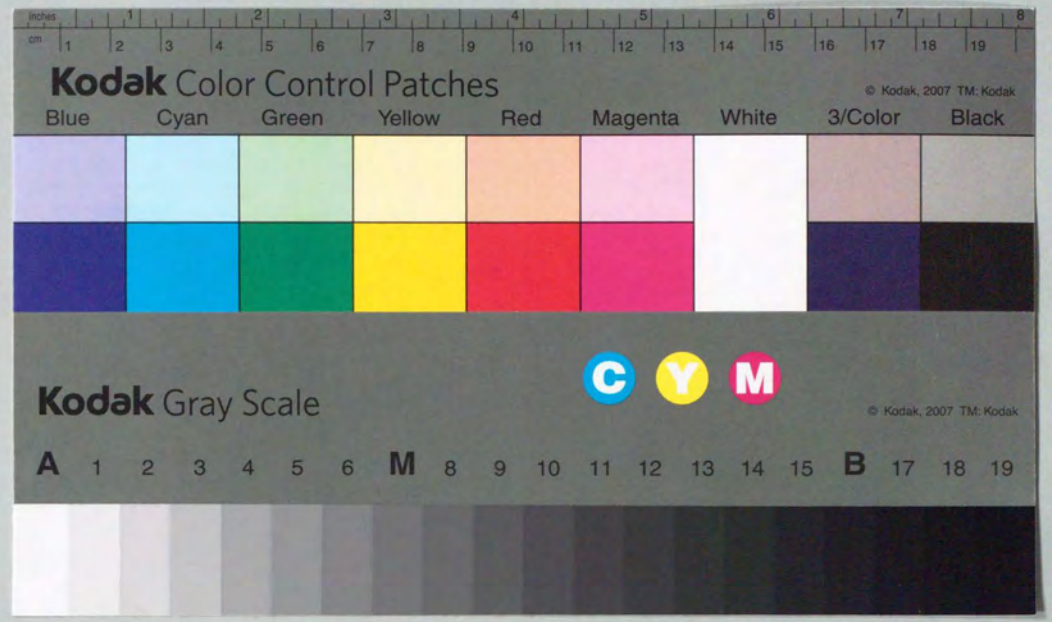
inches
cm
Kodak Color Control Patches
© Kodak, 2007 TM: Kodak
Blue
Cyan
Green
Yellow
Red
Magenta
White
3/Color
Black
C
Y
M
Kodak Gray Scale
© Kodak, 2007 TM: Kodak
A 1 2 3 4 5 6 M 8 9 10 11 12 13 14 15 B 17 18 19